FEBRUARY 2025

IN COMPLIANCE™

THE COMPLIANCE INFORMATION RESOURCE FOR ELECTRICAL ENGINEERS

Was it the Radar?

Respectfully Revisiting the 1967 US Navy USS Forrestal Carrier Disaster

INCLUDING

- Tailoring MIL-STD-461 RE102
- A Circuit Model for the Charged Device Model Spark
- Expert Insights
- EMC Concepts Explained
- Hot Topics in ESD
- Troubleshooting EMI Like A Pro

WHO SAYS YOU CAN'T HAVE IT ALL?

and with next-day, on-time delivery

Preamplifiers
20 MHz - 40 GHz
8 Models

Low Loss Cables
DC - 40 GHz
4 Models

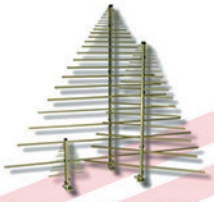

Log Periodics
80 MHz - 7 GHz
13 Models

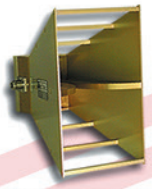

DRG Horns
170 MHz - 40 GHz
6 Models

H-Field Rods
100 Hz - 30 MHz
4 Models

Biconicals
20 MHz - 330 MHz
5 Models

All in one small package

Probes
20 Hz - 1 GHz
16 Models

BiLogicals
25 MHz - 7 GHz
8 Models

Loops
20 Hz - 30 MHz
7 Models

Standard Gain Horns
1 GHz - 40 GHz
9 Models

Tripods and Accessories

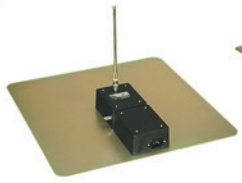

Monopoles
100 Hz - 60 MHz
5 Models

You Can Have It All when it comes to EMC/EMI testing. A.H. Systems is proud to bring you exciting new products, and many reliable favorites for your evaluation and compliance applications. Our antennas are unique and distinctive with broadband frequency ranges between 20 Hz up to 40 GHz. This enables us to specialize in various sales, rentals and, re-calibrations of test Antennas throughout the world. To view our products and get quick answers to your questions, access our comprehensive online catalog. Search for various information about product descriptions, typical AF plots, VSWR, power handling capabilities and links to product data sheets. Or simply request a catalog be sent to you. Not only have we been developing EMI Antennas for over 30 years, we also have organized worldwide sales representation. You can find your local knowledgeable representative in over 27 countries via our website. For quality products, excellent service and support with **next-day, on-time delivery.**

Antennas... **And Kits too.**

Innovation **Quality** **Performance**

Phone: (818)998-0223 ♦ Fax (818)998-6892
http://www.AHSystems.com

A.H. Systems

AMETEK®
COMPLIANCE TEST SOLUTIONS

RETHINKING SOLID-STATE AMPLIFIERS

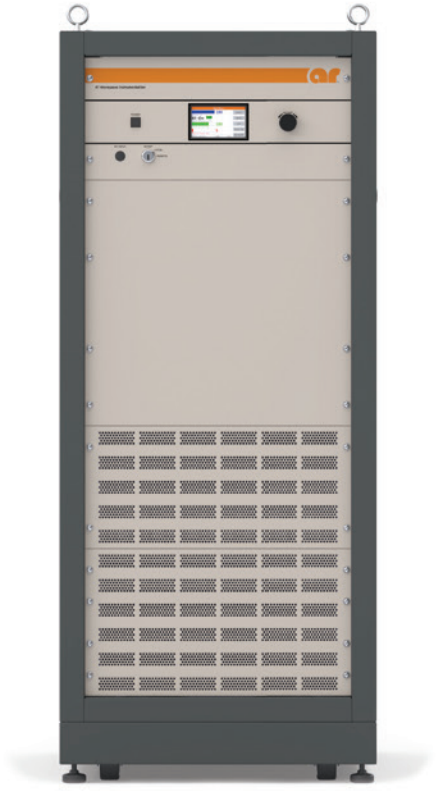

Think you know the application limits of a solid-state amplifier?

THINK AGAIN!

When it comes to pushing the boundaries of technology and ensuring the reliability of electronic systems, high power solid state amplifiers play a pivotal role in a growing number Aerospace & Defense applications:

- **HIRF (High-Intensity Radiated Field) Testing**
- **NEMP (Nuclear Electromagnetic Pulse) Testing**
- **EW (Electronic Warfare) Jamming and Jamming Simulation**
- **Component Testing**
- **EW (Electronic Warfare) Destruction**
- **Radar and radar simulation**

Visit us at www.arworld.us
Contact us at ari-sales@ametek.com or telephone 215.723.8181

Download the "Why Think Solid-State" infographic for a deep dive into the evolution of solid-state amplifiers!

THE POWER OF 3

emtest / TESEQ / ar

AMETEK®

MASTER COMPLIANCE **CHALLENGES WITH EXPERT GUIDANCE!**

IN COMPLIANCE BLOG SERIES

Expert Insights

Exclusive guidance from engineers like you.

A variety of expert perspectives on compliance design and testing, covering topics like EMC, EMI, and product safety.

Crack the Code to Compliance with Tips from Engineering Pros

Practical Engineering with Don MacArthur provides actionable insights on key compliance topics like uncertainty analysis, PCB spacing, and electrical insulation systems to help engineers streamline development and excel in compliance engineering.

In ***Product Insights***, Don MacArthur dives deep into practical EMI mitigation challenges, offering solutions for capacitor behavior, ferrite selection, differential probes, and more to optimize designs and advance engineering careers.

Ken Wyatt's ***EMC Bench Notes*** helps engineers identify and resolve EMC issues early in the design cycle using in-house pre-compliance testing tools, enhancing troubleshooting skills and reducing costly testing failures.

Patrick Andre's ***Military and Aerospace EMC*** shares valuable insights into EMC challenges in high-stakes environments like defense, aerospace, and military systems, offering engineers practical solutions and expertise.

Karen Burnham's ***Standards Practice*** explores immunity standards and advanced testing methods, helping engineers navigate compliance challenges in industries like defense, aerospace, and automotive with techniques like reverberation chamber testing.

Kimball Williams' ***Signals and Solutions*** connects the foundational techniques of amateur radio, such as Morse code, to modern EMC engineering, offering fresh perspectives on troubleshooting, testing, and innovation.

Full Collection of Blogs, Posts and Author Bios:
https://incompliancemag.com/expert-insights

Susbcribe here

Weekly updates on compliance engineering, including '*Expert Insights*,' are featured first in The In Compliance Weekly Newsletter.

IN COMPLIANCE

IN COMPLIANCE

FEBRUARY 2025

Volume 17 | Number 2

In Compliance Magazine
ISSN 1948-8254 (print)
ISSN 1948-8262 (online)
is published by

Same Page Publishing Inc.
451 King Street, #458
Littleton, MA 01460
tel: (978) 486-4684
fax: (978) 486-4691

FEATURE ARTICLES

COLUMNS

DEPARTMENTS

FCC Issues Final Rules for Program-Originating FM Boosters

The U.S. Federal Communications Commission (FCC) has adopted final rules that will provide FM radio stations greater flexibility in customizing content reaching different portions of their service areas.

So-called FM booster stations allow broadcasters to differentiate the programming that they air to certain geographic sections within their entire service areas. Originally used primarily for rebroadcasting transmission signals to areas where reception is poor, booster technology has now evolved to the point that broadcasters can use boosters to customize programming content delivered to different parts of their service area and air programming different from their primary station. However, until now, the FCC has limited advanced booster technology for use only on a temporary or experimental basis.

A Second Report and Order issued by the FCC now opens booster technology for broader use, including the use of program-originating boosters that allow broadcasters to provide listeners with more targeted content, such as localized weather reports and advertisements from local businesses.

FDA Issues Pilot Program to Enhance Medical Device Recalls

The Center for Devices and Radiological Health (CDRH) of the U.S. Food and Drug Administration (FDA) is launching a pilot program to help speed the release of news and information regarding potentially high-risk medical devices.

The FDA's pilot program will provide both consumers and industry with early alerts regarding the recall of potentially high-risk medical devices used in connection with cardiovascular, gastrorenal, obstetrical or gynecological, and urological issues. The goal of the pilot program is to minimize the time between when the FDA becomes aware of a potential device safety concern and the communications from the agency to the public regarding the safety concern.

The pilot program follows recommendations from the Patient Engagement Advisory Committee (PEAC) on how the FDA's recall efforts could be enhanced to reduce the time between FDA awareness of device-related risks and the communications with the public about those risks, their potential impact and actions that can help minimize those risks.

More FCC Fines for Pirate Radio Operators in Boston Area

The Enforcement Bureau of the U.S. Federal Communications Commission (FCC) is continuing its active pursuit of illegal radio operations, announcing the latest round of fines against pirate radio operators.

A total of $200,000 in forfeiture penalties have been issued in connection with three pirate radio operators based in Brockton, Massachusetts, including $120,000 against Renold David, $40,000 against Djovany Pierre and Mario Turner, and $40,000 against Joao Vieira.

According to the Commission, its efforts over the past four years to increase enforcement efforts against illegal radio broadcasting have resulted in more than $14.5 million in proposed fines and over $5.5 million in penalties.

FCC Modifies Emissions Limits to Align with WRC Requirements

The U.S. Federal Communications Commission (FCC) has modified emissions limits applicable to frequency bands used for certain mobile operations to align its requirements with those of other national telecommunications authorities.

According to a Report and Order, the Commission has modified its rules for the 24.25-24.45 GHz and 24.75-25.25 GHz bands to align with a Resolution passed in 2019 by the World Radiocommunication Conference (WRC-19). Specifically, the FCC has aligned the requirements detailed in Part 30 of its rules for mobile operations in these frequencies with the limits set forth in WRC-19 Resolution 750.

Currently, the 23.6-24.0 GHz band is allocated for use by certain passive scientific and research services, including the Earth Exploration Satellite Service (EESS), essential to meteorological applications such as weather forecasting. According to the FCC, its rule changes are intended to protect the 23.6-24.0 GHz band from unwanted emissions that could adversely impact its use.

Researchers Efficiently Convert Heat to Light

To help create a safer and less toxic energy storage alternative to batteries, a group of researchers at Rice University are actively exploring the development of a super-efficient storage technology that efficiently converts heat to electricity.

According to an article posted on the website of Interesting Engineering, the researchers are working to develop a high-efficiency thermal emitter, one that absorbs heat and converts that heat into electromagnetic radiation. The electromagnetic radiation is then captured by a photovoltaic cell to generate electricity.

The researchers say that the use of a thermal emitter can help to reduce energy loss during the conversion of heat to electricity, a critical limitation of current thermophotovoltaic (TPV) systems used for heat-to-electricity conversion.

A Circuit Board Grown from Leaves??

As the world struggles to get control over the rapid escalation in the growth of electronic waste, a group of scientists may have come up with an innovative natural solution that could significantly increase the production of biodegradable electronics.

Researchers at Dresden University of Technology (TU Dresden) have developed a biodegradable electronic circuit board made from tree leaves. Instead of using fiberglass or composite plastic, which are difficult to recycle, the research team assembled a webbed skeleton of leaves to create a substrate. The substrate was then dipped into ethyl cellulose, a biodegradable polymer, resulting in a smooth, flexible, and transparent material that can handle high temperatures comparable to nonrecyclable plastics.

At the end of their predicted useful life, the "leaftronic" substrates can then be placed in an ultrasonic acid bath and eventually degrade after about a month in compost.

EMC BENCH NOTES

Interpreting Emissions Using a Near-Field Probe

By Kenneth Wyatt

Most engineers are familiar with near-field probes and that they are sensitive to E- or H-fields emanating from circuit boards, cables or enclosure seams. They are really the first order of business when evaluating a circuit board or system. A more advanced characterization technique is to not only identify the major energy sources, but to interpret different emission types observed. That's the purpose of this article.

Figure 1: A typical near-field probe set. In this picture, there are three H-field loop probes and one E-field probe.

Figure 1 shows a standard set of four probes from Beehive Electronics. The pointed one is an E-field probe, while the three circular examples are H-field probes in various loop diameters.

A set of near-field probes may be obtained from many other sources, including Aaronia AG, Com-Power, Langer EMV-Technik, Rigol, Rohde & Schwarz, and Siglent.

SELECTING THE RIGHT PROBE

When would you use an E-field probe versus an H-field probe?

Circuits that produce a fast-changing voltage are usually higher-impedance circuits and so tend to produce a dominant E-field. You'll typically find this at the switch node of DC-DC converters or in the high voltage switching loop of an off-line power converter. E-fields are also produced within leaky enclosure seams.

Circuits that produce a fast-changing current are usually lower-impedance, so they tend to produce a more dominant H-field. Examples include most circuit traces on PC boards or interconnect cables. Because H-fields typically dominate in PC boards, I tend to use an H-field probe to characterize emissions of various sources.

Why typically three sizes of H-field loops? It boils down to sensitivity and field pick-up resolution. The larger H-field probe is most sensitive to detecting H-fields but has lower resolution; that is, it's more difficult to "zero in" on particular circuit traces that may be carrying noise currents. The smallest diameter H-field probe can resolve noise currents down to specific traces in many cases, but the sensitivity is low enough that you may need a broadband preamplifier to boost the signals for better observability.

Probing around on PC boards and cables can reveal the major EMI sources of harmonic energy and is always a good first step. But many designers may have trouble progressing from that point and really understanding what it is they're seeing and what to do next.

BROADBAND VERSUS NARROWBAND

I introduced the broadband (BB) versus narrowband (NB) concept in "How to Use Spectrum Analyzers for EMC" (*In Compliance Magazine*, November 2024, and I'd like to dig a little deeper now. First, we need to better understand the difference between BB and NB harmonic emissions. Second, we need to realize that whether harmonic signals are considered BB or NB depends on the EMI receiver or spectrum analyzer receiver passband (that slice of frequency spectrum to which the analyzer is responding, often referred to as resolution bandwidth (RBW)). See Figure 2 for clarification.

The traditional definition of broadband is a signal that produces "noise" across a wide band of frequencies. For example, thermal noise from a resistor or "shot" noise from a semiconductor junction will produce a continuous band of energy across a wide range of frequencies. In the audio world, this might be called "white" or "pink" noise.

The more likely cause on product designs today is fast-changing digital or power converter circuits. A good example is an

on-board DC-DC converter that switches at only 1 MHz but has switching edge speeds (rise-/fall-times) of 1 to 3 ns or less. These fast edges create a broad spectrum of harmonic energy as high as 2 GHz.

A narrowband signal in the traditional sense would be observed as discrete harmonic "spikes," and you'd see one or more depending on the RBW setting of the spectrum analyzer.

In Figure 2, if the total energy of the harmonic being observed fits within the RBW, then it's considered narrowband. If the harmonic energy is wider than the RBW, it's considered broadband. This might seem to be a little odd in that the narrowband/broadband classification depends on how the measurement gear is set, but the basic concept is that broadband signals are wider than the receiver bandwidth (or RBW).

Figure 3 shows a combination of BB and NB emissions. Understanding how to interpret these emission profiles helps to identify the circuit causing it. What appears to be a rise in the measurement noise floor and tapering down gradually is considered a BB emission, while the series of narrow spikes is considered NB.

For the example above, I chose an RBW of 30 kHz for argument's sake. We're looking from 10 to 800 MHz with a log-frequency horizontal axis, which I tend to prefer, as it is quicker to identify particular frequencies.

Harmonic energy sources that produce a broad increase are generally created by fast-switching DC-DC converters. You'll also see a broad rise in emissions from digital switching of address and data buses, often with NB spikes riding along. To visualize the envelope clearly, requires the use of MAX HOLD mode and waiting for the analyzer to perform multiple sweeps to fill in the gaps. Note that a real-time spectrum analyzer will not generally require multiple sweeps to record a clear BB signal.

What's very interesting is that if we were to reduce the RBW down to a narrow 300 Hz to 1 kHz, we'd be able to resolve the DC-DC converter switching as a series of NB spikes separated by the converter switching frequency (typically 100 kHz to 3 MHz nowadays). This demonstrates that whether a harmonic signal is considered BB or NB, depends on the RBW setting of the analyzer.

So that we don't get bogged down in interpreting whether a signal is considered BB or NB, the EMC standards always define the measurement RBW depending on the frequency band being measured. For example, in the non-military world, we generally use Table 1. For MIL-STD, we replace 9 and 120 kHz with 10 and 100 kHz.

In fact, unless you elected to get the "EMI Option" for your spectrum analyzer, you may not be able to select the 9/120 kHz RBW settings. Just use 10/100 kHz, instead, as that is close enough for troubleshooting or debugging efforts.

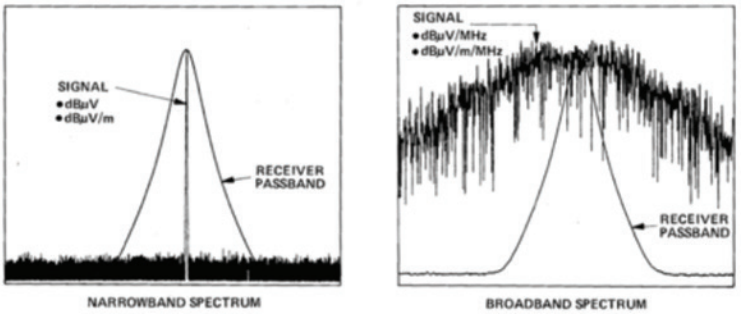

Figure 2: Idealized example of a narrowband signal, which fits within the resolution bandwidth (receiver passband) and a broadband signal whose energy does not fit within the receiver passband. Diagram, courtesy Hewlett-Packard.

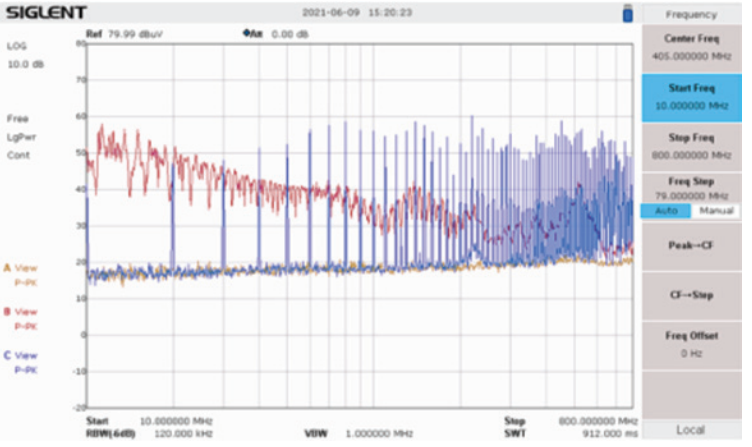

Figure 3: There are two common types of high frequency harmonics: narrowband (in the blue trace) and broadband (in the red trace). MAX HOLD mode was used to help reveal the envelope of the BB emission. The yellow trace is the ambient noise floor of the measurement system and is always used to document a measurement system baseline or noise floor.

RBW	Freq Band
9 kHz	9 kHz to 30 MHz
120 kHz	30 to 1000 MHz
1 MHz	>1 GHz

Table 1: Resolution bandwidth versus frequency according to most commercial EMC standards.

EXAMPLES OF EMISSION PROFILES

The ability to interpret the emission profile of various harmonic energy sources will greatly help in tracing back to the source and beating down radiated or conducted emission challenges for your product. For example, when I see a family of NB spikes, I immediately think of a digital clock. If I see a BB profile, I immediately suspect an on-board DC-DC converter or digital bus noise currents.

By characterizing the dominant harmonic energy sources in advance, you should be able to take the observed radiated or conducted emissions and backtrack to the source. All examples below are using an RBW of 120 kHz, and I usually find the middle-sized H-field probe to be best.

Figures 4 through 6 demonstrate examples of harmonic profiles I've commonly seen for different on-board sources. These emission profiles should be carefully recorded for comparison to emission failures during pre-compliance or compliance testing.

Figure 4 is a frequency sweep from 10 to 1000 MHz, showing an example of a narrowband 48 MHz fundamental clock with harmonically-related spikes every 48 MHz. This can be confirmed by subtracting the frequencies from any two adjacent spikes. Using a log frequency sweep helps to visually identify frequencies.

In Figure 5, and sweeping over the same frequency range, we see an example of broadband digital bus noise with narrowband clock spikes riding on top. The peaking around 400 MHz could indicate a cable and/or board resonance. Note that it's common to have a combination of narrowband emissions riding along on top of a broadband emission.

In Figure 6, we're now sweeping from 150 kHz to 1 GHz, and we observe typical broadband DC-DC converter noise. This was captured using MAX HOLD mode. The broad peak from 200 to 300 MHz is likely due to cable and/or PC board resonances. This self-generated EMI can couple to sensitive wireless receivers and cause lack of sensitivity.

SUMMARY

By first identifying the major energy sources and characterizing their emissions profiles, it is possible to correlate particular conducted or radiated emissions with the source or sources on the PC board (or within the system) that could be the root cause. Future Bench Notes will bring in additional tools and probes to help this process.

REFERENCE

1. Wyatt, *Workbench Troubleshooting EMC Emissions*, Volume 2, Chapters 3 and 4.

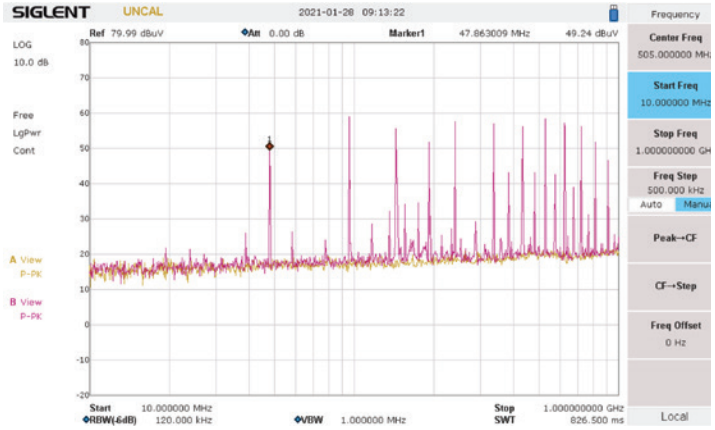

Figure 4: Narrowband clock. The yellow trace (not very visible in this case) is the measurement noise floor.

Figure 5: Broadband digital bus noise. The yellow trace is the measurement noise floor.

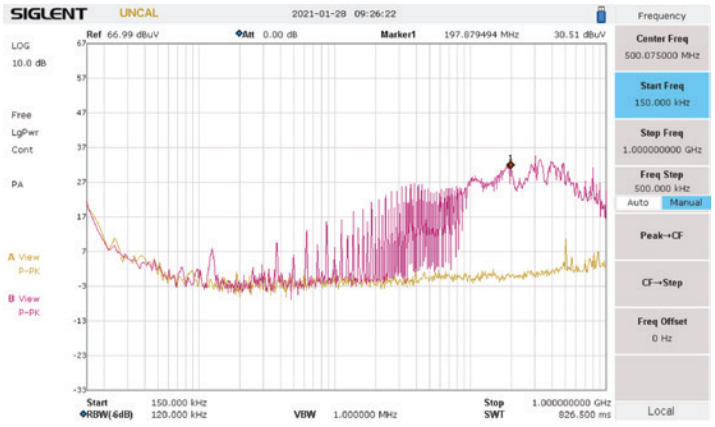

Figure 6: Broadband DC-DC converter noise. The yellow trace is the measurement noise floor.

PRACTICAL ENGINEERING

Creepage Distance of an Optocoupler

By Don MacArthur

This month's blog is pulled from the product safety playbook. It highlights a potential issue to avoid when considering an optocoupler's creepage distance when placed onto a printed circuit board (PCB).

Recall that the purpose of an optocoupler is to provide isolation of the hazardous voltages present on one side of a circuit from reaching the non-hazardous elements on the other side of the circuit, and creepage distance is the shortest distance along the surface of a solid insulating material between two conductive parts (IEC 60664-1:2020).

If the proper creepage distance is not maintained, then not only is there a potential safety issue with the end-product resulting in the product failing NRTL certification (and the subsequent delay to releasing it to production), or worse, the issue going un-noticed and placing product in the field that has a potential safety issue.

POLLUTION DEGREES

Recall that pollution in the micro-environment is a parameter to consider when evaluating creepage distances. There are four degrees specified (pollution degrees 1 through 4). We will only consider pollution degree 2 here, where only non-conductive pollution occurs, except that a temporary conductivity caused by condensation is to be expected occasionally. This condensation may occur during periods of on-off load cycles of the equipment.

WORKING VOLTAGE

The RMS voltage applied to the circuit is also used to determine the required creepage distance. This voltage is the highest value of the steady-state working voltage (see 4.2.5 of IEC 60664-1:2020), the rated insulation voltage, or the rated voltage.

MATERIAL GROUP

Material group also affects determination of creepage distances, and materials are classified into four groups according to their comparative tracking index (CTI) values.

- Material Group I is the best with 600 ≤W CTI
- Material Group II is second best with 400 ≤ CTI < 600
- Material Group IIIa is 175 ≤ CTI < 400
- Material Group IIIb is the worst with 100 ≤ CTI < 175

"THE" POTENTIAL ISSUE

Based on a pollution degree 2 micro-environment, working voltage requirements for the end-product, and material group for components found in the circuit, including the optocoupler and PCB, assume we determined that we need to use an optocoupler with a minimum of 8 mm of creepage distance. We review specifications online and find a suitable component with the correct NRTL safety approvals. Everything is good to go, right? The correct answer is almost, but not completely. Consider what would happen if the parts placement diagram for the part was incorrect and the pads on the PCB shortened our required 8mm creepage down to just 7.2 mm, as shown in Figure 1.

As the note in the figure states, "PCB pad to pad only requires material group I creepage, while the copper pads common with the optocoupler reduces the effective creepage distance for the optocoupler's material group IIIx surface."

CONCLUSION

Initially, everything was done right by selecting an optocoupler with the proper 8 mm creepage distance based on pollution degree, working voltage, and material group. However, once placed onto the PCB, the placement method violated spacing rules, and only 7.2 mm creepage was obtained. Placing copper pads in a way that reduces the required creepage distance is something to avoid, not only in regard to optocouplers but other safety-critical components as well.

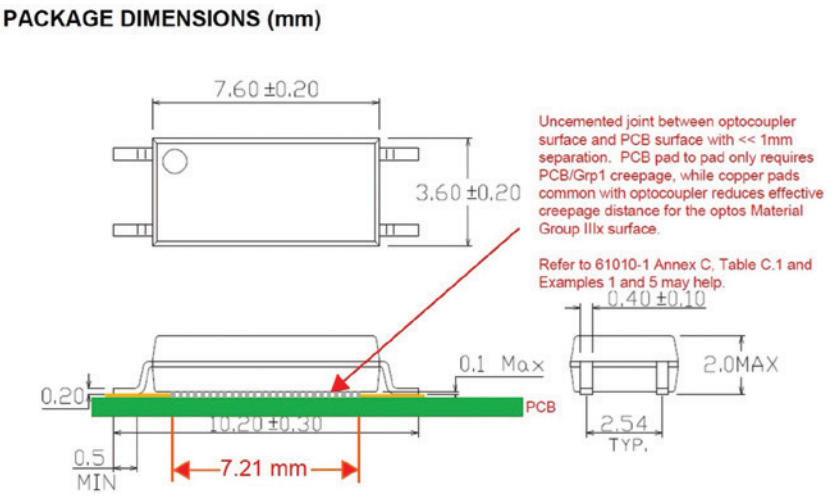

Figure 1

MILITARY AND AEROSPACE EMC

Why and How We Use LISNs

By Patrick André

First, the Line Impedance Stabilization Network, or LISN (pronounced "listen"), is not intended to be a filter. Although it can function as a bit of a filter, please do not use it in this manner. The original intent was to simulate the line impedance found on aircraft power lines. The work was first performed by Alan Watton, who worked on the Douglas DC-3 type aircraft during WWII.[1] This was originally a 5 µH LISN design, which the RTCA and most aircraft manufacturers still use. The LISN has been used in military and aerospace testing since the early 1953's. The 5 µH LISN was first used in MIL-I-6181B (29 May 1953). It was also used in DO-138 (1967) and may have been used earlier.

This ubiquitous use of LISNs has provided another benefit, which I believe is more important: The use of a standardized test setup and power line impedances allows testing to be performed and replicated at different testing laboratories and hopefully find the same or similar results. When everyone uses the same source line impedance, cable lengths, ground planes, and standoffs, the ability to reproduce the emission measurements provides assurance that the results can be trusted. [2]

Earlier versions of DO-160 included the schematic for the LISN, whereas DO-160D and later versions included only the impedance curve, with a note stating that a 10 µF capacitor may be needed on the power line side of the LISN to achieve the low frequency impedance required. The modified schematic is shown in Figure 1.

The MIL-STD 461D-G LISN (see Figure 2) has a slightly different design and includes a 50 µH inductance. The effect of the larger inductor is to provide a 50 Ω impedance to a lower frequency. Note that while conducted emissions for DO-160 start at 150 kHz, MIL-STD 461D-G starts at 10 kHz.

Conducted emission measurements made for DO-160 are performed starting at 150 kHz and use a current probe on the power line, although early versions allowed measurements directly from the LISN port. Note that the port provides a voltage measurement, while the current probe provides a current measurement (to state the obvious). However, the two may not directly relate. Increased line impedance may increase the measured voltage but decrease the measured current. For this reason, only one method was chosen for testing.

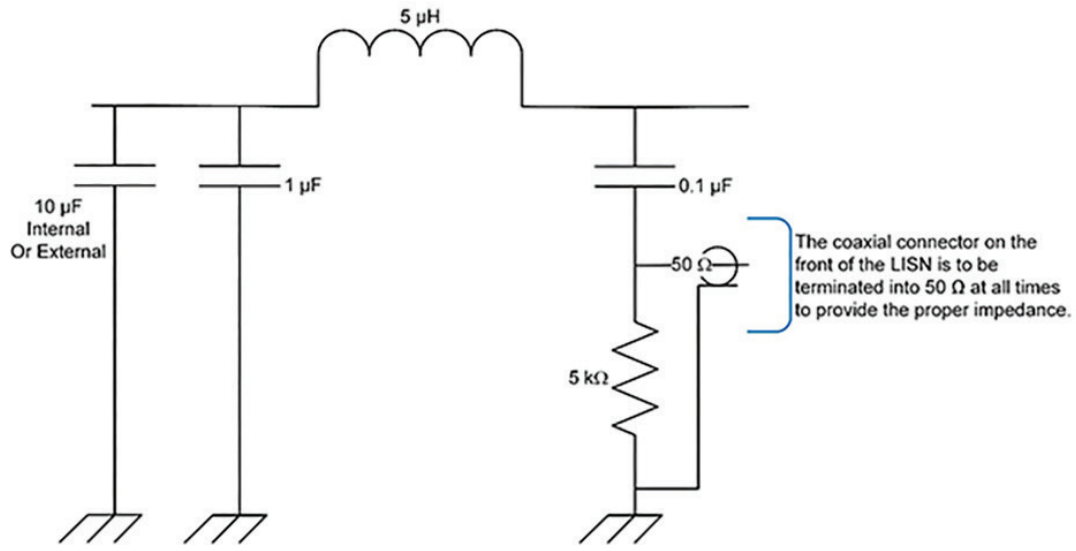

Figure 1: The DO-160 LISN included the additional 10 µF capacitance required of later versions

For MIL-STD 461A-C, current emission measurements were made on all lines using a current probe, but on power lines, this was problematic. At the time, most agencies required the use of 10 µF capacitors on the power line instead of LISNs. However, the capacitor has less than 1 Ω impedance above 16 kHz. With the approximately 1.5 µH of series inductance in the 1 meter input wire, resonances were often a problem, and a filter using capacitors as a first stage was rendered inefficient. Thus, starting with MIL-STD 461D, LISNs were used on power lines. Conducted emissions were voltage measurements made at the port of the LISN and starting at 10 kHz. Due to the low frequency, the 50 µH LISN was used to extend the impedance down in frequency.

For power supplies that provide power to the aircraft bus, it is important to use LISNs on the output of the power supply. This is often neglected. But remember, the intent is to replicate the aircraft bus impedance, and the LISN is the device we have chosen to do this.

Secondly, the coaxial connector port of the LISN must always be loaded into a 50 Ω load, either using a terminator or a measurement device (spectrum analyzer). And ensure the load is rated for the power it needs to handle. For high-level conducted susceptibility testing (DO-160 Category Y, MIL-STD 461 Level 5), the test levels can be up to 600 mA (6 dB over test levels). If 0.6 Amps of current has to pass through the 50 Ω termination, this results in having to dissipate 18 Watts. Some current may pass through other components, but a significant amount of current must run through the termination. If only a ½ Watt termination is used, as is often done, the termination will fail, and the test will be invalid. The currents must be allowed to flow from the line to the ground plane and back to the unit, and the path is mostly through the termination. Please ensure the termination is large enough to handle the required current.

ENDNOTES

1. This information was provided by the late Al Parker to Ken Javor. Details can be found in Mr. Javor's excellent article "Line Impedance Stabilization is in its Seventieth Year and Still Going Strong," *In Compliance Magazine*, June 2023.
2. Arguments can be made if the limits are realistic and should be modified. That is not the point of this article, only that the ability to reproduce the findings makes them trustworthy.

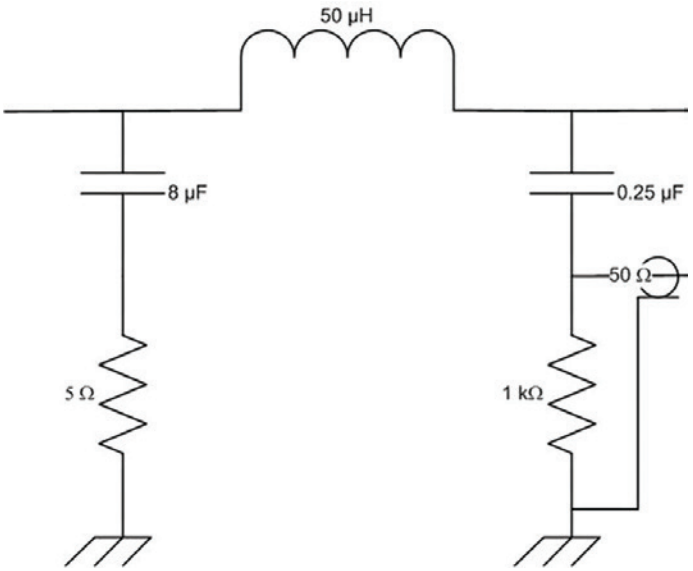

Figure 2: The MIL-STD 461D-G LISN

WAS IT THE RADAR?

Respectfully Revisiting the 1967 US Navy USS Forrestal Carrier Disaster

Part 1

Dr. Brian Kent is an engineering consultant and adjunct professor at Michigan State University. His 37-year USAF career included roles as the Chief Technology Officer (AFRL), Chief Scientist (AFRL Sensors Directorate) and Senior Scientist for Low Observable Technology. He supported NASA's Columbia investigation and Shuttle missions, holds multiple IEEE fellowships, and received a Presidential Rank Award. He's passionate about naval aviation history. Kent can be reached at brian.kent.phd@gmail.com.

By Brian M. Kent, Ph.D.

In 1967, while on patrol in the Gulf of Tokin, the United States Navy Carrier USS Forrestal was executing wartime missions over North Vietnam. At 10:45 AM local time, the ship was preparing to launch more than 27 A-4 Skyhawk and F-4B Phantom Fighter jets, all fully fueled and armed with a mixture of iron bombs, precision missiles, and Zuni rocket launchers. At 10:51 AM, an F-4B experienced an un-commanded Zuni missile launch on the flight deck, striking a neighboring A-4 and starting a fire causing a series of devastating secondary explosions. Quenching the fire nearly capsized the ship, which was ultimately saved through the heroics of the sailors who served aboard the Forrestal.

Although the US Navy conducted an extremely thorough accident investigation, many follow-up technical articles in the aerospace and NASA literature, including current EMI design books, blamed the initiation event on EMI from on the on-board AN/SPS-43 VHF search radar. This article is aimed at reinforcing the official USN record regarding the accident's true root cause. The Forrestal's many "lessons learned" led in part to the creation of an entirely new discipline called "insensitive munitions" within the Electromagnetic Compatibility community and is therefore a critical event to understand.

DEDICATION

This article is humbly dedicated to the families, relatives, and friends of the 134 Sailors killed and 167 severely wounded on July 29, 1967 aboard the USS Forrestal. We honor the hundreds of additional survivors who suffered from a lifetime of PTSD and "survivors' guilt." The bravery and heroics of the Sailors who saved the USS Forrestal and its 5,400 lives by quenching the fire and preventing the carrier from capsizing cannot possibly be overstated.

On July 29th, 1967 the Navy Carrier USS Forrestal (CVA-59) experienced one of the most tragic accidents in the modern US Naval aviation history. While preparing to launch a 27-plane strike mission into North Vietnam, an un-commanded Zuni rocket was launched on deck from an F-4B fighter, striking an A-4 Skyhawk aircraft across the deck, causing an initial fuel-fed fire. Within 94 seconds, huge secondary explosions rocked the carrier launching one of the most devastating fires in US Navy history since the Second World War. This accident and the lessons the US Navy learned from it completely changed everything about modern US Naval aviation from fire-fighting to launch procedures to designing weapons to be hardened from electrical faults and direct contact with fire.

The 1967 Forrestal accident investigation *correctly identified* the root causes of the fire. However, over subsequent years researchers and engineers began to insert or augment their own perspectives, biases, and conclusions about the fire which upon close inspection are in direct conflict with the original Forrestal accident conclusions. Several citations and alternate history myths have only grown over the years to the point that original root causes were either lost or highly distorted. To illustrate, I have randomly chosen three such references.

In July 1995, a NASA EMC Design book produced by NASA's Marshall Space Flight Center [1] published the following version of the Forrestal accident and its conclusions (note the underlined text below is the author's emphasis):

> *"In 1967 off the coast of Vietnam, a Navy jet landing on the aircraft carrier U.S.S. Forrestal experienced the un-commanded release of munitions that struck a fully armed and fueled fighter on deck. The results were explosions, the deaths of 134 sailors, and severe damage*

to the carrier and aircraft. This accident was caused by the landing aircraft being illuminated by carrier-based radar, and the resulting EMI sent an unwanted signal to the weapons system. Investigations showed that degraded shield termination on the aircraft allowed the radar frequency to interfere with routine operations."

In 2006, Clayton[2] updated a foundational EMC Design book for the IEEE. On page 13 in the introductory chapter is this reference to the USS Forrestal fire:

"On July 29th, 1967, the USS Carrier Forrestal was deployed off the east coast of North Vietnam. The carrier deck contained numerous attack aircraft that were fueled and loaded with 1,000 lb. bombs, as well as air-to-air and air-to-ground missiles. One of the aircraft missiles was inadvertently deployed, striking another aircraft and causing an explosion of its fuel tanks, and the subsequent death of 134 service people. The problem was thought to be caused by the generation of radio frequency (RF) voltages across the contacts of a shielded connector by the ship's high-power search radar."

In 2008, an IEEE EMC briefing published by Joffe [3] had the following observations about the Forrestal accident:

"On July 29, 1967, USS "Forrestal" cruised off the coast of North Vietnam. Its jets had already flown more than 700 sorties and there was no reason to expect this day to be any different. Not threatened by enemy aircraft, the A4 "Skyhawks" on the deck were loaded with fully fueled two 1000 lb. bombs, air to ground and air to air missiles. Somewhere on the deck of that carrier, attached to the wing of an aircraft, was an improperly mounted shielded connector. As the RADAR swept around, RF voltages generated on that cable ignited a missile which streaked across the deck, striking an aircraft and blowing its fuel tanks apart. Its two 1000 lb. bombs rolled to the deck and exploded."

Having a lifelong interest in US Naval aviation history, I decided to use my experience from my service with the Columbia Space Shuttle Accident Investigation Board to revisit the USS Forrestal accident. As I poured through mountains of online and written source material from the Forrestal investigation, it became very evident that an old quote attributed to Mark Twain was applicable – "*It ain't what you know that gets you into trouble. It's what you know for sure that just ain't so.*"[4] To understand what happened that day, we need to learn fundamental carrier operations from 1967, beginning with the design and operation of the USS Forrestal itself.

THE USS FORRESTAL AND AIR OPERATIONS IN PEACE TIME

The USS Forrestal (CVA-59, Figure 1) was commissioned in 1955 as the lead ship in the Super Carrier class. The US Navy had learned a great deal from trying to operate various jet aircraft from WW2-era Essex-class straight deck aircraft carriers, and realized a major redesign of aircraft carriers for jet operations was required. The Forrestal was thus the first carrier designed exclusively for jet operations.

Figure 1: US Navy Carrier USS Forrestal (CVA-59) with its ship logo (inset) [5]

EXODUS ADVANCED COMMUNICATIONS

Where Defense & EMC Solutions Begin!

Amplifiers
CW & Pulse

RF & Microwave Amplifiers
10 kHz-75 GHz

EMC
APPLICATIONS

AMP2083P-2KW
4.0-8.0 GHz

AMP4022DBP-LC-2KW
8.0-12.0 GHz

AMP2080-LC-10KW
10 kHz-250 MHz, 10,000W

MILITARY
APPLICATIONS

COMMERCIAL
APPLICATIONS

EXODUS
ADVANCED COMMUNICATIONS

MPA1081
1-18 GHz, 1W

AMP2074P-2KW
1.0–2.5 GHz, 2KW

MPA1003
2.0-8.0 GHz, 2W

3674 E. Sunset Road, Suite 100, Las Vegas, Nevada 89120 USA
Tel : 1-702-534-6564 Email : sales@exoduscomm.com

www.exoduscomm.com

Watch the deck crews carefully during the launch and landing or recovery operations. Consider all the dangerous tasks that must be completed by the deck crews even under peacetime or training operations. If you served on a carrier deck crew, you knew that injuries and fatalities were commonplace.

The ship was 1,067 ft. in length, 238 ft. in beam, and drafted 37 ft. of water. The ship was a floating city, with a complement of 552 officers, and 4,988 enlisted sailors. It was the first USN carrier with an angled deck (a Royal Navy innovation), four steam catapults, and a radial optical landing system to improve deck landing safety. The Forrestal could carry and perform air operations with 85 jet aircraft of various types. In 1967, these types included the Phantom F4-B, the A-4 Skyhawks, E-2C Hawkeye radar plane, S3-B Vikings, A3 Sky Warriors, and various helicopters. The Forrestal was not nuclear-powered like her later cousins, as its engines were powered by oil-fired boilers. The bunker fuel oil on board had important implications later in the 1967 accident.

When the McDonnel Douglas F-4B Phantom jet became operational with the US Navy in 1963, the USS Forrestal was the first carrier to host an F-4B squadron. If the reader is not familiar with flight operations on a flight deck of this historic era, some important background is required to understand both the complexities and dangers of working around a flight deck. Since print media does not offer a good way to visualize complex carrier operations, I have posted a short US Navy video of the F-4B operations on the USS Forrestal from 1963. To assist in understanding the rest of this article, I strongly suggest watching it to provide context (https://youtu.be/2LDPKwS91s8).[6]

Watch the deck crews carefully during the launch and landing or recovery operations. Consider all the dangerous tasks that must be completed by the deck crews even under peacetime or training operations. There are many inherent flight deck dangers associated with moving jet tugs, steam catapult cables, jet blasts, etc. If you served on a carrier deck crew, you knew that injuries and fatalities were commonplace. Also note that, in this video, none of the aircraft shown have armed and operational weapon systems, although several of the pictured F-4Bs had external fuel tanks.

If you ever encounter a sailor who has served as one of the colored deck shirt crews on a carrier, you would soon learn of the dangers. One sailor interviewed had the following perspective:

> *"The most dangerous job is having a job on the flight deck. I was a green shirt aboard the USS Nimitz. I have seen an F-18 crash, a helicopter crash, (and) almost got sucked into an F-14 intake, as well as blown across the deck and plenty more close calls. I attribute my attention to detail and situational awareness today to my time spent on the flight deck."*

So, what do those carrier deck shirt colors represent? The **Red** jerseys were the ordinance and explosive handlers, and disposers. They were also assigned to crash and salvage operations. The **White & White-Checkered** jerseys were responsible for aircraft inspections, squadron readiness inspectors, as well as on-deck medical and safety personnel. The **Purple** jerseys handled everything related to the JP-5 aviation fuel, including fueling, defueling, and fuel integrity. The **Brown** jerseys were "Plane Captains," responsible for general maintenance and moving specific aircraft around on deck.

The last three jersey sets had the most dangerous jobs on deck. The **Green** jerseys were responsible for handling the bridle, executing catapult attachment and, upon landing, detaching the arresting gear. The **Blue** jerseys were aircraft handlers, elevator operators, as well as tow and start cart drivers. Lastly, the **Yellow** jerseys (or "mini-air Bosses") were the plane directors and aircraft handling officers assigned to each of the four catapults. They were the sailors who gave the final command to launch.

TYPICAL CARRIER MUNITIONS AND SAFETY PROTOCOLS IN 1967

While USN jet aircraft were regularly flying with radar-guided Sparrow missiles and infrared-guided Sidewinder missiles in Vietnam, munitions that were

used against ground targets in Vietnam were largely iron bombs in the Mark 82/83/84 family. Figure 2 shows the Mark 82/83/84 family, courtesy of the National Museum of the USAF. [7] Normally the USN A-4 Skyhawk and F-4B Phantom jets would carry and drop the Mark 82-84 iron bombs. These weapons were not armed on the deck of a carrier when the aircraft were catapulted. During a strike, after the bomb was released from the aircraft, the spinners shown in Figure 2 (inset) would spin for 10-15 seconds before the weapon was fully armed[8]. This gave plenty of time for the weapon to separate from the aircraft before exploding. Also, if any of the Mark 82-84 weapons were put in direct contact with a deck fire, the casings and internal materials had specifications to survive for up to 5-10 full minutes in direct contact with fire *without detonating!* This important point will become relevant shortly in the fire's root cause.

Figure 2: Mark 82/83/84 Vietnam-era iron bombs of yield 500/1,000/2,000 lbs. (Courtesy NMUSAF) [7]

On 24 July 1967, the USS Forrestal was spending its first full day on "Yankee Station" 60 miles off the coast of North Vietnam, after having sailed around the world from Norfolk, Virginia. On 25 July 1967, the Forrestal rendezvoused with the US Navy ammunition ship Diamond Head (AE-19) to obtain ordinance for upcoming strikes against North Vietnam. At this time, due to high mission rates against North Vietnam, there was a Pacific theater-wide shortage of Mk83 (1,000 lb.) bombs. Since the MK83s were the weapon of choice for the A-4 Skyhawk, missions would have to be cancelled if the MK83s were not available.

The Diamond Head was a logistics vessel assigned through the US Navy Systems Command, and therefore decided to supply the USS Forrestal with 26 aging Korean War era AN-M65A1 1000 lbs. bombs[9] (Figure 3) instead of the Mark 83's. When these 26 bombs were transferred to Forrestal, there was an immediate uproar from the Forrestal's munition's safety officer. The munitions squadron was extremely upset about the poor condition of the AN-M65A1 weapons, many of which were rusting, and several were leaking contents. Apparently, the Diamond Head had picked these weapons up from ammo dumps in the Philippine Islands and was supposed to transport them back to the States for disposal. In their poor condition, the Diamond Head likely transferred these weapons to Forrestal to get rid of them.

The Forrestal's weapons officers refused to place these 26 weapons below deck in the armored weapons storage deep within the ship. The officers petitioned Forrestal's Captain John Belling to immediately throw all 26 weapons overboard. Capt. Belling requested the skipper of the Diamond Head to remove the bombs, but Diamond Head replied that these 26 1,000 lbs. bombs were the only ones available for missions that week. Captain Belling reluctantly directed that all 26 AN-M65A1 bombs were to be stored on the armored flight deck in the "bomb dump" just aft of the carrier's island. He also ordered strike planners to use these 26 weapons on missions as quickly as possible.

This decision had momentous implications since the AN-M65A1 were "thinned-skinned" bombs that were not rated to survive direct exposure to fire. Historically, these weapons were known to explode in ~50-80 seconds with direct fire contact, and sometimes faster!

Figure 3: Korean Era AN-M65A1 1,000 lb. "Thin-Skinned" bomb[9]

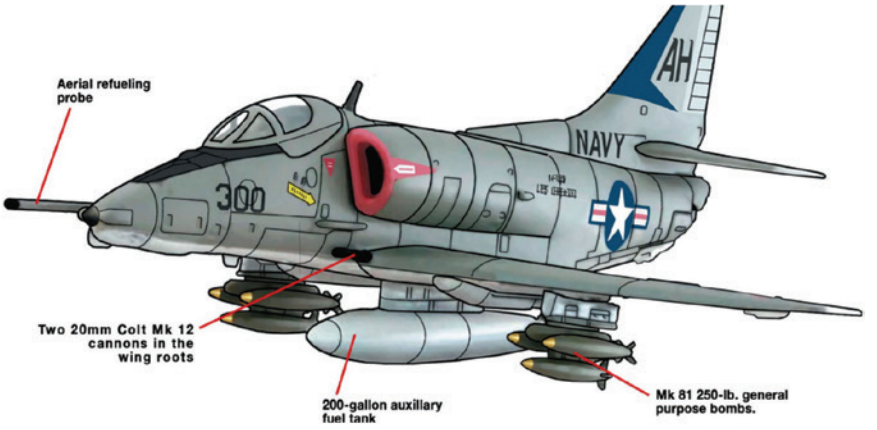

Figure 4: McDonnel Douglas A-4 Skyhawk equipped with a 200-gallon JP-5 tanks and 6 Mk81 250 lb. bombs [10]

Figure 5: Jet ground start cart on Carrier USS Constellation connected to and starting an A-4 Skyhawk [11]

BACKGROUND ON THE MCDONNEL DOUGLAS A-4 SKYHAWK AND F-4B PHANTOM JETS

Let's discuss in more depth two of the most important combat aircraft used for ground attack missions on the USS Forrestal, the A-4 Skyhawk, and the F-4B Phantom. The McDonnel Douglas A-4 Skyhawk was a single-seat ground attack and fighter (see Figure 4). This A-4 is equipped with one 200-gallon JP-5 external fuel tank and 6 each of Mk-1 250 lb. bombs.

On July 29, 1967, five A-4s scheduled for launch at 1100 that morning were loaded with one 400-gallon JP-5 centerline tank and 2-each of the AN-M65A1 1,000 lb. bombs. Unlike the "shacked" bombs shown in Figure 4, the old Korean era AN-M65A1 bombs were "slung-hung" on the A-4s using specialized canvas straps which were released when the bomb was dropped. These straps were also to play a role later in the day.

On 29 July 1967, the USS Forrestal had planned to launch three different combat strike missions. One mission was to launch at 0700, the second at 1100, and the third at 1500. To get rid of the 26 old AN-M65A1 bombs, the plan was to send 10 bombs out on five A-4s with the 0700 strike. Ten more bombs would go with the 1100 strike using five A-4s, and the remaining six AN-M65A1 bombs would be used on the 1500 strike using three A-4s. The hope was to get these volatile weapons off the ship by the end of the day on 29 July 1967.

The A-4 Skyhawk, like most jets of its era, required a specialized ground cart to start the engines before being launched. Figure 5 shows a typical USN carrier ground start cart connected to an A-4 on the carrier USS Constellation. Generally speaking, it took several minutes to start the engines from the ground start cart. Once the engines were up to speed, the pilots switched over their main power from the ground start to internal aircraft power. Starting an A-4s was therefore a well-known and safe routine.

The F-4B Phantom was a much more complex combat weapon system, capable of carrying a wide range of munitions, and having the ability to fly at sustained supersonic speeds. The F4-B joined the US Navy in 1963, and the "Bedeviler" squadron, seen on the carrier video earlier, was deployed with the

USS Forrestal in July of 1967. With its twin turbojets, the F4-B also required a "ground start cart" similar to the A-4 cart shown in Figure 5. Figure 6 shows an Air Force F4 connected to an Air Force version of a ground start cart.

To fully understand the root cause of the Forrestal accident, we need to thoroughly explore the procedure to start an F-4B Phantom jet from a ground start cart. Let's begin by examining the F-4 cockpit controls shown in Figure 7.[13] The F-4B was normally started with the assistance of a ground start cart shown in Figure 5. To protect the F4-B's own power generating system during startup, the aircraft's electrical systems were switched over to run on the ground cart's power. The F-4B cockpit switches to accomplish this are shown on the right in Figure 7. The switches would be placed in the ground start cart EXT position for both the right and left engine power systems. In this position, the pilot would start his engines, one at a time, and make sure they were fully spooled up and wouldn't flame out.

Normally during this process, the pilot has his *left hand* on the two engine throttles shown in Figure 7 on the left side, while his *right hand* would remain on the switch positions. In order for the pilot to disconnect his aircraft electrically from the ground start cart, he would simultaneously switch the two right switches from the EXT position to the L-Gen/R-Gen position. In doing this, his

Figure 6: A USAF F4 Phantom with a ground start cart [12]

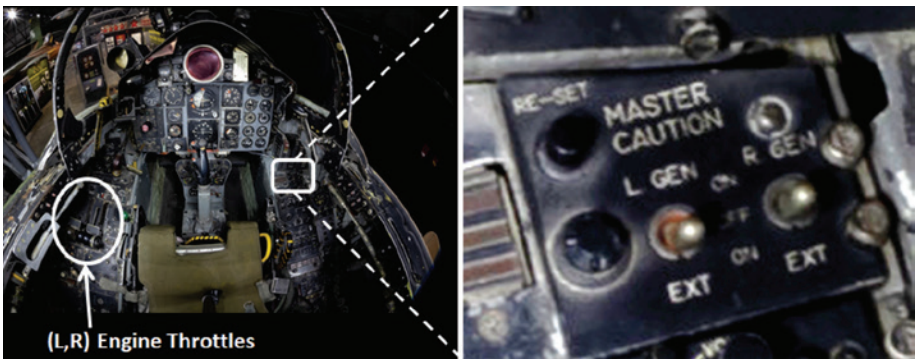

Figure 7: F-4 showing two power toggle switches used to switch aircraft power from a ground start cart (EXT or LOWER position) to the left or right aircraft engine generator (L Gen/R Gen-Upper position) [13]

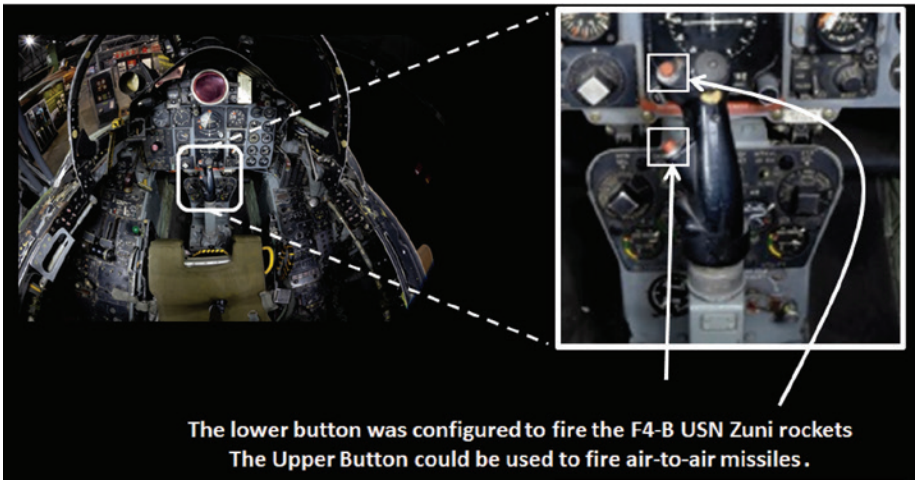

Figure 8: F-4 cockpit showing a close-up of the control stick and weapon stations trigger (firing) buttons [14]

right hand would NOT be on the control column stick, and his *left hand* would remain on the engine throttles.

Looking at the actual control column itself, we can also understand the controls necessary toggle one of the many weapon systems installed on the F-4B. Figure 8 shows a close-up of the control column itself with two of the firing or trigger buttons. Since the F-4 had multiple-weapon stations for bombs, Zuni rockets, and air-to-air missiles, the pilot could select which firing button triggered which weapon though, for the Zuni rockets, the lower buttons were typically-selected.

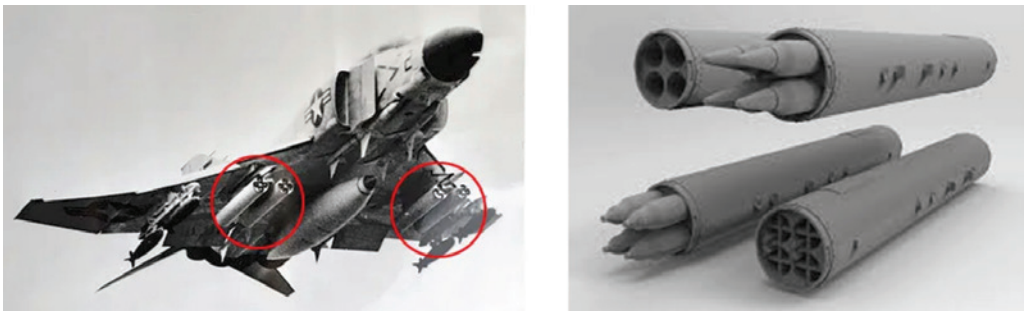

Figure 9: (L) An F4-B with two LAL-10 launchers each controlling two 4-tube 5" Zuni rockets (R) [15,16]

THE LAL-10 LAUNCHER AND ZUNI ROCKET SUBSYSTEMS

Next, let's examine the 5" Zuni rocket system as it was typically installed on USN F-4B's at the time. Figure 9 [15,16] shows an F4-B carrying both iron bombs and four 5" Zuni missile launchers as connected to two LAL-10 weapon stations. These four pictured Zuni tubes could

each carry four 5" rockets for a total load-out in this picture of 16 rockets. Each of the unguided Zuni's carried 125 pounds of high explosive, and were generally used to suppress enemy air defense positions.

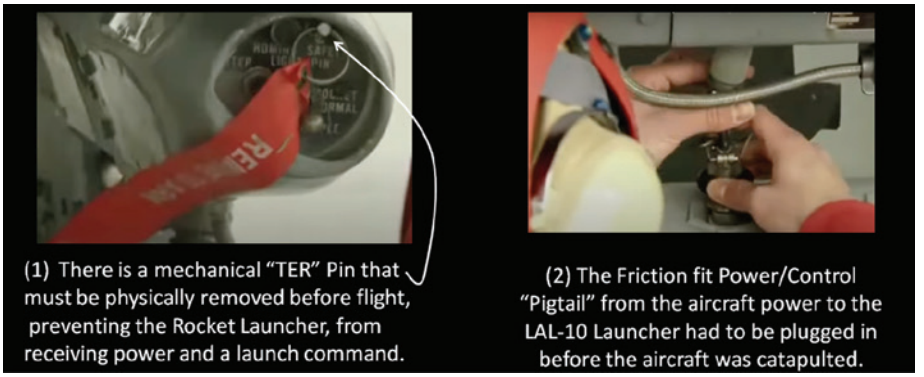

Figure 10: LAL-10 Launcher TER safety pin and friction fit power/control "pigtail" [17, 18]

How did ground safety handle these weapon systems to prevent them from going off while the aircraft was on the ground? In the case of the Zuni rocket launchers, the F4-B Zuni launch design was supposed to be impervious to an accidental launch of the Zuni *except in the air and in a combat situation*. In particular, the USN F4-B weapon system design supposedly required six different interlocks to be closed in order to actually fire any weapon, including the Zuni. Three of those interlocks resided in the cockpit. The pilot had to: 1) select the Zuni weapon station; 2) engage the cockpit weapon master arm switch; and 3) push the appropriate control stick trigger.

The fourth interlock was the landing gear doors. If the gear doors were open, as one would expect on deck, a landing door interlock switch was supposed to prevent launching the weapon if the landing gear doors were open. The last two weapon safety interlocks occurred on the LAL-10 launcher that held the Zuni rockets themselves. These two safety interlocks are shown in Figure 10.

On the back end of the LAL-10 launcher was a "TER" safety pin with a red "remove before flight" flag. The TER pin was designed to push an internal LAL-10 switch for both the power and the firing pins into an interrupted or shorted position. In other words, if somehow a firing command had overridden the remaining four interlocks discussed above, this TER pin was supposed to be the safety measure of last resort. This safety pin was supposed to be pulled from the LAL-10 launcher *at the catapult, in the seconds before the jet was catapulted into flight*.

In addition, the right pigtail friction fit power and firing line connector had to be attached. This pigtail connected the aircraft power and all firing path connections between the F4-B and the LAL-10 launcher. If someone forgot to plug this pigtail in before flight, none of the weapon systems controlled by the LAL-10 would be functional. *This connection was also supposed to be done at the catapult*, hence the friction-fit nature of the quick disconnect connector.

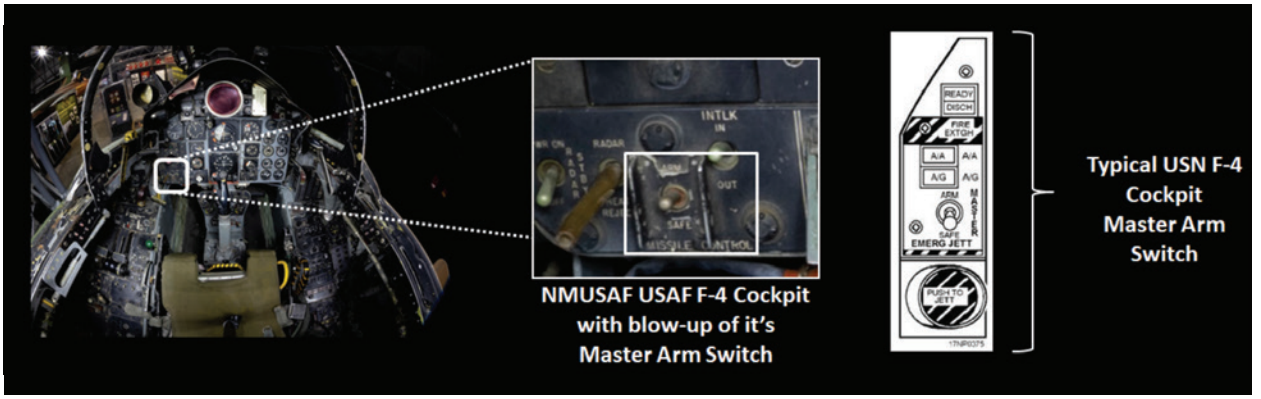

Figure 11: Close-up of the "master arm" weapon station switches in USAF F-4 and USN F4-B [19, 20]

With these six interlock systems in place, the USN Systems Command's official engineering position was that "*it (would be) impossible to accidentally fire a weapon controlled by the LAL-10 on the deck.*"

Let's return for a moment back to the master arm and weapon station interlocks. Again, using the NMUSAF cockpit photograph, the USAF version of the master arm switch is shown in Figure 11. However, the USN's F4-B master arm and weapons emergency jettison cockpit switches had a slightly different configuration as shown on the far right of Figure 11. Again, during aircraft start-up, the pilot's hands were on the throttles (left hand) and the external power to generator switches (right hand), and nowhere close to the master arm or jettison switches.

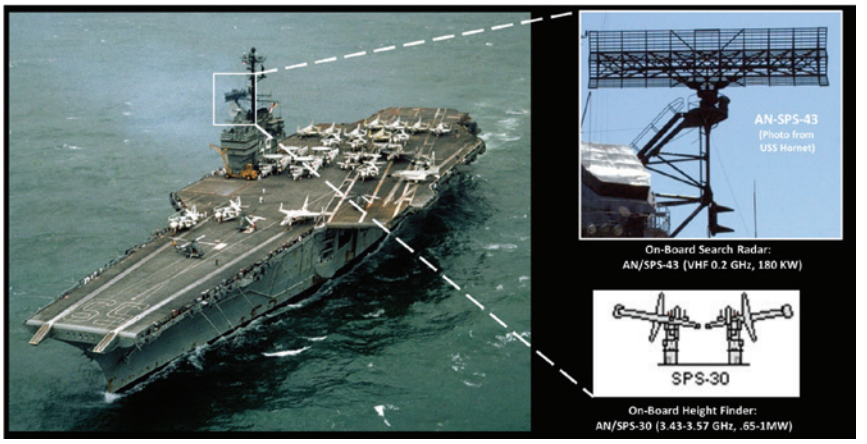

Figure 12: USS Forrestal's AN/SPS-43 and SPS-30 radars [21,22]

USS FORRESTAL'S RADAR SYSTEMS AND PLATS CAMERA SUBSYSTEM

Let's introduce the current on-board high-powered radar systems of the USS Forrestal, shown in Figure 12. The Forrestal's combat information system was built around the two radars shown. The larger of the two was the AN/SPS-43 long range search radar which operated at 200 MHz, at a peak transmit power of 180 Kilowatts. The antenna pattern was narrow in the azimuth plane, and a broad fan in the elevation plane. Theoretically, it could detect air targets out to 500 km and sea skimming targets to 30 km. The AN/SPS-43 radar was augmented with an S-band SPS-30 height-finding radar, whose function was to get weapons grade range and elevation tracking information for ship self-defense purposes. The SPS-43 would provide a cue to the SPS-30. In addition, the SPS-30 was used during aircraft carrier launch operations to monitor the individual launch velocity of the aircraft being catapulted to ensure the aircraft had sufficient velocity to prevent it from stalling. The SPS-30 velocity information was digitally provided to the pilot landing aid television system (PLATS), which will be discussed shortly.

As mentioned in the introduction, catapulting and trapping an advanced jet aircraft onto a carrier was considered the most skilled and dangerous flying operation in the entire US military. To ensure every pilot was "on top of their game," the USN installed the PLATS camera system on the Forrestal in 1963 (see Figure 13). The purpose of the PLATS system was to film (or videotape) every single carrier aircraft launch and landing. Pilots would be graded on how well they executed their takeoffs and especially their landings.

When "trapping" or landing, the pilots had to catch one of four arresting cables on deck using their tail hook. A perfect landing was hitting arresting cable #2. If a pilot consistently came in too fast and hit #1 or overshot and hit #4, their proficiency was downgraded. If they couldn't improve and hit #2 consistently, they lost their carrier pilot certification.

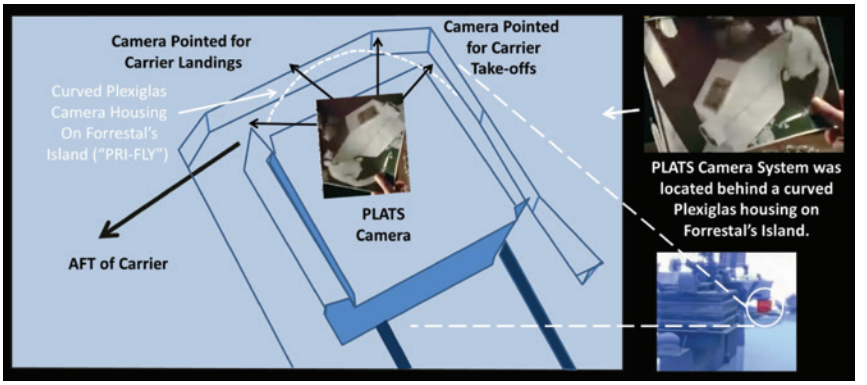

Figure 13: Pilot landing aid television system (PLATS) camera and operator location on USS Forrestal [23]

The most important takeaway here is that the PLATS camera was constantly filming every takeoff and landing, and this system would play an outsized role in recording the subsequent accident. To see a typical PLATS video from the USS Forrestal, please visit https://youtu.be/VuCe73IJD7U. Note that the original Forrestal PLATS system recorded *the exact time of day to second accuracy* **and** *the exit velocity of the launched aircraft* from the Ships SPS-30 radar, to ensure the catapult was launching the aircraft well above its specified stall speed.

WARTIME CARRIER OPERATIONAL VARIATIONS OF THE USS FORRESTAL ON JULY 29, 1967

With the essential technical background laid, we now turn our attention to the Forrestal on July 29, 1967. The carrier had been on Yankee station in the Gulf of Tonkin for four days, and the plan for the day was to conduct three separate attack strikes with three groups of the Forrestal's air complement. Now on a wartime footing, it is clear that the launching and recovery operations had increased in pace, size, and danger. Forrestal had trained extensively for this day, but there were some very notable differences between their training and actual combat operations. For instance, as discussed above, the A-4 and F-4B always started their engines well before their turn on the launch catapult, in order for the engines to be well warmed up and ready for full throttle needed at takeoff. Also, the red shirt weapons technicians were regularly measuring voltage surges on F-4B subsystems at the moment the pilot switched from the ground start carts to their internal 400 Hz aircraft generators.

To avoid any possible "electrical glitch" prior to making the final LAL-10 launcher weapons connections, the approved procedure during training was for the red shirt weapons personnel to make the final weapons pigtail connections and remove the TER safety pins *at the catapult* just before launch, as shown earlier in Figure 10. If this were done in haste, as frequently happened during the launch of large combat raids, pigtail electrical pins could and were frequently bent, therefore subject to potential shorts in future connections. The real problem, however, was that the Vietnam pilots and their squadron commanding officers complained that making these connections at the catapult significantly slowed down the rate of aircraft launches, and inhibited aircraft recoveries. Connecting all the weapons pig tails could add minutes to each launch depending on the A-4 and F-4B weapons loadout and the size of the strike.

During their transit from Norfolk to the Gulf of Tonkin, the flight deck crews on the Forrestal were briefed by previous Pacific Command carrier weapon handler crews that they had created an ordinance safety "work-around." In essence, to speed up launches, the red shirt munitions pigtails were to be attached well before arriving at the catapult, and frequently before the aircraft engines had been started. Furthermore, the Forrestal's red shirts and their munition officer supervisors indicated that this procedure had been approved "by waiver" by previous Pacific Fleet Carrier captains. With this waiver in place, the Forrestal red shirt deck crews were now *solely reliant on the "TER safety Pin"* that, in theory, was designed to electrically and mechanically prevent a Zuni weapon launch command from the LAL-10 launcher unless the TER pin was pulled. So, the procedure was supposed to be that the red "remove before flight" TER Pins would be pulled at the catapult, while the power and firing line pigtail were already connected.

This is where the first inconsistency of practice took place. While the TER pin was supposed to be pulled out at the catapult, in large combat strikes *the TER safety pin was often removed prior to arriving at the catapult*. Furthermore, the red jerseys noticed that the TER safety pin had a very loose friction fit. During a launch, the deck winds were typically between 33-39 miles per hour. As related in post-accident witness statements, in several incidences the TER pin was dislodged completely and blown out by the deck winds alone. In the days preceding July 29, 1967, several TER pins and their red flags were seen on Forrestal's deck during post-launch "Foreign Object Damage"(FOD) sweeps of the flight deck.

Regarding the supposed "safety waiver" mentioned above. It turns out only Captain John Belling could approve such a safety waiver. A former decorated carrier aviator himself, Captain Belling later testified he was never notified of the pre-catapult LAL-10 pigtail connection and early removal of the TER safety pin before the catapult. In the subsequent investigation board, he stated that he would never have approved this new procedure. Reviewing

Captain Belling's many safety messages and "Family Grams" written and read to crew on the voyage from Norfolk to Yankee station, he clearly and consistently emphasized flight deck safety measures even over combat operational efficiency.[24]

It's now July 29, 1967. The fateful morning of the accident has finally arrived.

REFERENCES

1. Leach, R.D., and Alexander, M.B., Editor, NASA Reference Publication 1374 titled Electronic System Failures and Anomalies Attributed to Electromagnetic Interference, Marshall Space Flight Center, July 1995, pp 7, para 2.3.1.
2. Paul, Clayton R., *Introduction to Electromagnetic Compatibility*, Wiley, Second Edition, pp 1.3, page 13.
3. Joffe, Elya B., "Electromagnetic Compatibility (EMC) – an Evolving Discipline from the 'Garbage of Electronics' to Global Intersystem Compatibility A Historical Review with Personal Perspectives," Proceedings of the IEEE International Conference Microwaves, Communications, Antennas and Electronic Systems, COMCAS 2008, May 2008.
4. Attribution uncertain, but frequently attributed to Mark Twain.
5. Courtesy USN and National Archives, 31 May, 1962, KN-4507.
6. You Tube Archive Source. https://youtu.be/2LDPKwS91s8
7. Photo Courtesy of the National Museum of the United States Air Force (NMUSAF).
8. Saffold, Ray G., "Safe Arming Times for the Mk 81, 82, 83, 84, and M117 Low Drag Bombs," United States Naval Ordinance Laboratory Report NOTR-69-135, White Oak, Maryland, 1 August 1969.
9. Photo Courtesy: https://wiki.warthunder.com/AN-M65A1_Fin_M129_%281,000_lb%29#/media/File:M65A1_Fin_M129.png
10. Photo Courtesy: https://www.historynet.com/arsenal-4-skyhawk
11. National Geographic History Channel, Single Frame Grab from "Seconds from Disaster Aircraft Carrier Explosion," Original Broadcast 9-1-2021.
12. Frame grab from https://www.youtube.com/watch?v=rT_gLtwAjBs
13. Photo Courtesy NMUSAF https://media.defense.gov/2022/Feb/08/2002935433/-1/-1/0/220208-F-AU145-1011.JPG
14. Photo Courtesy: NMUSAF https://media.defense.gov/2022/Feb/08/2002935433/-1/-1/0/220208-F-AU145-1011.JPG
15. Photo Courtesy: http://www.revuair.com/2017/07/25/we-will-not-forget-3
16. Photo Courtesy: Pinterest https://www.pinterest.com/pin/pinterest--324048135678007426
17. National Geographic History Channel, Single Frame Grab from "Seconds from Disaster Aircraft Carrier Explosion," Original Broadcast 9-1-2021.
18. National Geographic History Channel, Single Frame Grab from "Seconds from Disaster Aircraft Carrier Explosion," Original Broadcast 9-1-2021.
19. Photo Courtesy: NMUSAF https://media.defense.gov/2022/Feb/08/2002935433/-1/-1/0/220208-F-AU145-1011.JPG
20. Photo Courtesy: https://navyaviation.tpub.com/14313/css/Armament-Safety-Override-Switch-364.htm
21. Courtesy USN and National Archives, 12 August 1967, Accession #: 330-CFD-DN-SC-04-09140.
22. Courtesy Wikipedia - Jon 'ShakataGaNai' Davis, https://en.wikipedia.org/wiki/AN/SPS-43#/media/File:SPS-43_radar_of_USS_Hornet_(CVS-12)_2008.jpg
23. Inset Camera Photo from National Geographic History Channel, Single Frame Grab from "Seconds from Disaster," Original Broadcast 9-1-2021, Original from US Navy PLATS Camera.
24. Killmeyer, Kenneth V., *Fire, Fire, Fire on the Flight Deck Aft; This Is Not a Drill*, Autherhouse Publishing 2018, Family Grams to Crew from Captain Belling, pp 82-85 and pp 85-88.

TAILORING MIL-STD-461 RE102

How to Focus RE102 Testing on the Things that Really Matter

Karen Burnham is the President and Chief Engineer of EMC United. She has over two decades of experience in the aerospace, defense, automotive, and other industries and is currently the Vice President of Standards for the IEEE EMC Society. You can reach her with any questions or discussion at karen@emcunited.com.

By Karen Burnham

MIL-STD-461 RE102 is probably the most commonly failed test in the aerospace/defense world, with 50-90% of units failing their first pass testing. This is a frequent cause of schedule delays, first for troubleshooting, and then for all the meetings needed to process waivers. There are ways that it can be tailored, even very early in the product development process, to minimize the need for waivers after test failures. Any time a unit fails a test but is allowed to move forward after going through a waiver process, it's an indication that the requirements were not set appropriately at the beginning of the program.

Ultimately, we want to do the minimum amount of testing that gives us the best assurance of mission success. We don't want to over test and jeopardize cost and schedule targets. But we also don't want to under test and miss something that could cause issues on the integrated platform. Understanding the purpose behind RE102 requirements helps us tailor them in a program-specific way.

RE102 exists primarily to protect *intentional RF receivers* on a platform from stray emissions from onboard electronics. If you look at the limit levels in MIL-STD-461 (Rev G is the most recent version at the time of writing), a typical value might be 69 dBμV/m. That equates to a field strength of 2.8 mV/m at 1 m. Generally speaking, not many non-RF electronics modules will be sensitive to that level of noise (consider the typical RS103 level of 20 – 200 V/m). Given the 1/r fall-off of field strength over distance, RF receivers not co-located with the unit will usually not react to these levels. It's the RF receivers installed along with the electronics that are most at risk from these high frequency but relatively low amplitude emissions. Thus, our RE102 limits should be tailored to the RF systems that will be present on the platform, if known.

There's a lot we don't know at the beginning of a program. We may not know exactly what radios will be selected, or which vendors will provide them. We may not know what antennas will be chosen, what their field of view is, where they will be placed, etc. However, we *do* know what kind of program we're working on: spacecraft/aircraft/marine/terrestrial. And we likely know what kind of RF systems will be required: UHF, GPS, S-band, Ka-band, air traffic control, special electronic warfare devices, etc. So even if we don't know our specific spectrum allocations yet, we can say "We will have receivers that will be using these frequency bands." Once we know that, we can focus our tailoring efforts appropriately.

SELECTING FREQUENCY RANGES

The first thing to look at is the frequency ranges to test. Here are the default frequency ranges from MIL-STD-461 Rev G, RE102:

- Ground 2 MHz to 18 GHz
- Ships, surface 10 kHz to 18 GHz
- Submarines 10 kHz to 18 GHz
- Aircraft (Army and Navy) 10 kHz to 18 GHz
- Aircraft (Airforce) 2 MHz to 18 GHz
- Space 10 kHz to 18 GHz

Testing at the lowest frequency range, 10 kHz – 2 MHz, should be done only in cases where there are onboard systems that are sensitive to very low frequency energy, such as antisubmarine warfare detection units. Otherwise, this frequency range should be omitted. As Ken Javor has noted elsewhere in the pages of this magazine, testing in this range is done in the near field, not the far field, and is messy and hard to reproduce.

If these VHF frequency ranges are important, consider using a common mode current measurement as an alternative, such as that described in GSFC-STD-7000B, Section 2.5.2.1.2. That will give you relevant information without the concerns about near-field vs. far-field antenna measurements.

The same can be said for the 2 – 30 MHz range (rod antenna) and 30 – 200 MHz range (biconical antenna). If you do not have any VHF receivers, consider skipping these ranges as well. They also have reproducibility problems, plus skipping two antenna configurations saves a good chunk of time. The fewer times you have to change antennas, the better. "Failures" in this range, without an intentional RF receiver in that range, are likely not relevant. (Obviously, there are other considerations that might come into play, such as if the unit or program is also required to meet CISPR 32 or EMCON limits.)

Here's a supporting quote from MIL-STD-461 Rev G, Section A.5.17:

> *"The 104 cm rod antenna [10 kHz – 30 MHz] has a theoretical electrical length of 0.5 meters and is considered to be a short monopole with an infinite ground plane. It would produce the true electric field if a sufficiently large counterpoise were used to form an image of the rod in the ground plane. However, there is not adequate room. The biconical [30 – 200 MHz] and double ridged horn [200 MHz – 1 GHz] antennas are calibrated using far-field assumptions at a 1-meter distance. This technique produces standardized readings. However, the true electric field is obtained only above approximately 1 GHz where a far field condition exists for practical purposes."*

If these VHF frequency ranges are important, consider using a common mode current measurement as an alternative, such as that described in GSFC-STD-7000B, Section 2.5.2.1.2. That will give you relevant information without the concerns about near-field vs. far-field antenna measurements. Testing can be done in a plain shield room without the need for a full semi-anechoic chamber (see Figure 1).

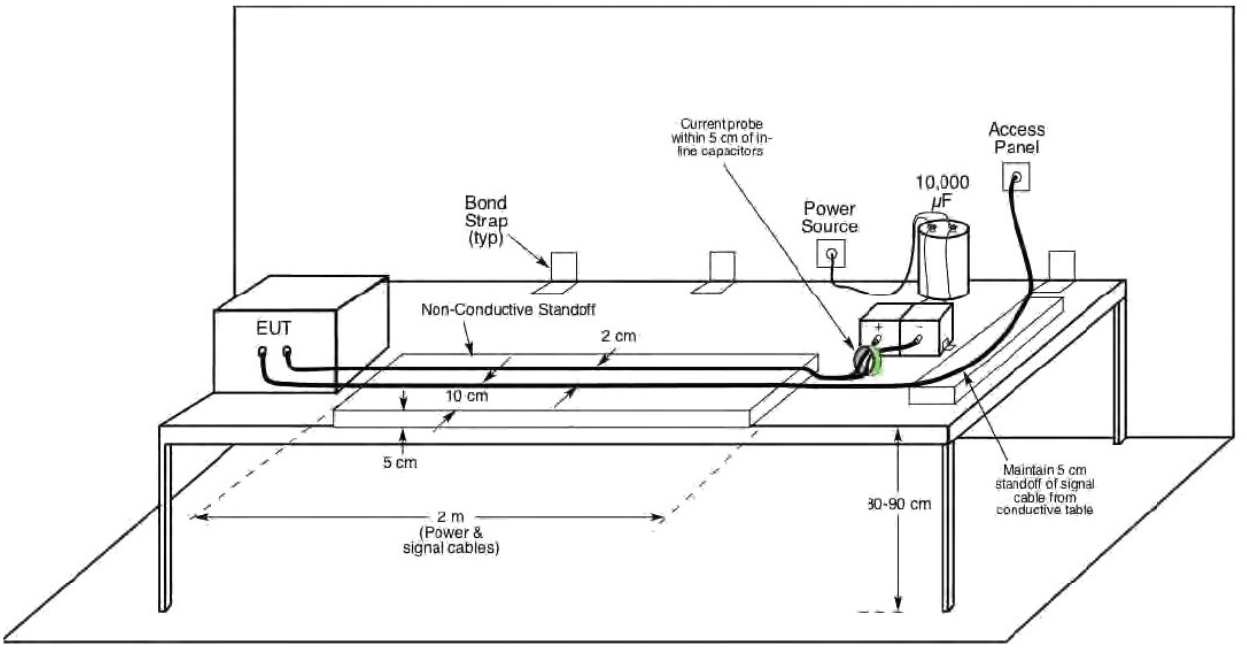

Figure 2.5-8. CMCE Test Setup, Modified CE101/CE03 Test Methods, Power Leads

Figure 1: Figure 2.5-8 from GSFC-STD-7000B depicting common-mode conducted emissions test setup.

This is a test method significantly different from the conducted emissions test methods found in MIL-STD-461 Rev G, which are differential mode measurements. The Goddard standard also calls for the use of an absorbing clamp rather than a typical clamp-on current probe. It has an extended argument for why this is a better approach in Section 2.5.3.3.2.4. I found the argument fascinating, and recommend that everyone give it some consideration.

Reining in the upper-frequency range is equally important. It is easily possible for the clocks of fast electronics systems to throw harmonics well into the GHz range. But if your highest frequency receiver is an S-Band comms system, do you need to test from 4 GHz – 18 GHz? Again, any "non-compliant" test results will likely be waived, since there is no on-board receiver that will suffer from the interference.

This is a good place for another caveat: receivers can be susceptible to interference outside their passband, both below and above it. It has been known to happen sometimes, that a spec sheet can misstate the out-of-band susceptibility of a radio receiver by 20 – 60 dB. Depending on the criticality of the system, you may need to start with very conservative assumptions of both sensitivity and susceptible frequency ranges, then relax the limits and/or narrow the frequency ranges when more about the potential victim system is known, either through analysis or test.

You may also need to "future-proof" your system. While you can be fairly sure a new RF receiver won't be added to a satellite after launch, the chances of new systems being implemented on an aircraft or naval vessel are much higher.

DESIGNING NOTCHES

Once you've identified which frequencies have receivers that need protection, you can calculate the minimum measurable field for each, without any knowledge of the specifics of the RF systems selected. (For the derivation that follows, I'm indebted to GSFC-STD-7000B, Section 2.5.3.3.7.4, with a few modifications.) We start with:

$$E = V_N + AF$$

At this point, we have drawn some very conservative notches that will flow down to the equipment designers as the program moves forward. This might not make everyone super happy, but you can just about guarantee that those limits will be relaxed up as the program evolves

Where E is the minimum detectable electric field strength in dBμV/m, V_N is the thermal voltage noise floor (dBμV), and AF is the antenna factor (dB/m). To calculate V_N:

$$V_N = -67\frac{dB\mu V}{Hz} + 10\log_{10} B$$

Where B is the bandwidth of the receiver (Hz). This equation is based on the theoretical noise power formulation, assuming a temperature of 290 K and a system with 50 Ω impedance. Then for the antenna factor:

$$AF = 30.22 + 20\ \log_{10} f - G$$

Where f is the frequency (GHz), and G is the gain of the antenna system (dBi). The constant also assumes a 50 Ω receiver system, so it should be adjusted if a different impedance is being used.

To get these equations, we've assumed a 50 Ω system at 290 K that's experiencing a free space plane wave (similar to the nominal test conditions for RE102). To calculate the minimum measurable field then, we need to know the bandwidth of the victim receiver, the frequency of the victim receiver, and its gain. We know at least the frequency range of the receiver from the system specs. We may not know the specific bandwidth of the system, but often there are standard bandwidths associated with things like GPS detectors. A close-enough guess is likely good enough for this initial limit.

Considering gain, do NOT use the main lobe gain of the receiver if it is known. You don't know much about either the receiver system or your electronics module under test, but you can be reasonably sure that it will not be installed in such a way as to block the main field of view of an RF receiver antenna. Instead, use the worst case of the sidelobes or back lobe of the antenna. Of course, if the antenna is intentionally omnidirectional, use the omni gain. If nothing is known about the system, 0 dBi is a conservative assumption.

At this point, we have drawn some very conservative notches that will flow down to the equipment designers as the program moves forward. This might not make everyone super happy, but you can just about guarantee that those limits will be relaxed up as the program evolves, instead of adjusted down at the last minute. (And no one seems to complain about relaxing limits!)

RELAXING NOTCHES

As the program progresses, there will be plenty of opportunities to revise these limits upward. One of the main ways comes once you have a better understanding of the overall construction of the platform. If all the RF receivers are on the exterior of a metal chassis (as is typical on aircraft and spacecraft, for instance), then electronics that are installed on the interior of the chassis can have their limits relaxed based on what is known about the shielding provided by the chassis.

Other parameters that you can include as they become available: the side lobe/back lobe gain of the specific receiver antennas; the out-of-band rejection performance of the RF receiver, and the noise tolerance

of the RF receiver, especially once the link budget has been determined. This initial tailoring analysis assumes that if *any* detectable signal is present, the RF system will be interfered with. That is likely untrue, and any knowledge about noise tolerance or error correction of the system should eventually be taken into account.

WHAT ABOUT THE OTHER FREQUENCIES?

What about the frequencies where we don't have any receivers? Let's say you have a UHF receiver at ~400 MHz, and a GPS receiver at 1.5 GHz, but not much in between. The safest thing to do is to use the default limits provided by MIL-STD-461 for your platform type in that middle-frequency range. The cheapest thing to do is skip 500 MHz – 1.4 GHz completely.

Another option would be to significantly relax the limit in the middle-frequency range. That way you still test it and can see if something is drastically wrong, for example, if the unit is throwing off levels of emissions that might interfere with neighboring systems either on or off the platform. But you won't call something a "failure" unless it is fairly extreme. Obviously, this will depend on the customer and the needs of the project. What the customer says they need and what they're willing to accept is usually the final word.

CONCLUSION

Is this kind of tailoring acceptable? Chapter and verse from the MIL-STD emphatically says "Yes":

> *"Possible tailoring by the procuring activity for contractual documents is as follows. The limits could be adjusted based on the types of antenna-connected equipment on the platform and the degree of shielding present between the equipment, associated cabling, and the antennas. For example, substantial relaxations of the limit may be possible for equipment and associated cabling located totally within a shielded volume with known shielding characteristics. It may be desirable to tailor the frequency coverage of the limit to include only frequency bands where antenna-connected receivers are present. Some caution needs to be exercised in this regard since there is always the chance [new] equipment will be added in the future. For example, it is not uncommon to add communications equipment (such as HF radio) onboard an aircraft as different missions evolve."* – MIL-STD-461G Sec A.5.17

This gives me an excuse to issue my standard (if you'll pardon the pun) reminder: Always Read the Appendices! For those standards that have them, informative and normative appendices and annexes often contain golden nuggets of wisdom that help the new user figure out how best to apply the standard. They are included by the standard's working group specifically to give context and guidance—and those working groups benefit from the collective experience of the careers of their members, sometimes a couple of centuries worth if you add up everyone's resumes. You're doing yourself a disservice if you don't give them a read-through whenever you're applying a new-to-you standard.

ENDNOTES

1. *General Environmental Verification Standard (GEVS) for GSFC Flight Programs and Projects*, GSFC-STD-7000B, 2021.

2. K. Javor, "(Re)Discovering the Lost Science of Near-Field Measurements – Part 1," *In Compliance Magazine*, July 1, 2023.

3. *Requirements for the Control of Electromagnetic Interference Characteristics of Subsystems and Equipment*, MIL-STD-461, 2015.

A CIRCUIT MODEL FOR THE CHARGED DEVICE MODEL SPARK

Understanding Reactive Elements in the ESD Plasma

Timothy J. Maloney is a Fellow of the IEEE and the co-author of the book, Basic ESD and I/O Design (Wiley, 1998). Maloney spent much of his 40-plus year career as a Senior Principal Engineer at Intel Corporation and has made numerous presentations at the annual EOS/ESD Symposia and other IEEE conferences. He can be reached at tjmaloney@sbcglobal.net.

By Timothy J. Maloney

The JEDEC/ESDA charged device model (CDM) test standard JS-002 places a component in a metal/dielectric test fixture and uses a field-induced air discharge to test each pin of the component. Current waveforms depend on the circuitry under test, yet are fairly consistent for the small and large CDM verification targets, metal disks specified by JS-002. Those waveforms often fit a simple 2-pole RLC circuit model as shown in Figure 1, and as summarized in our 2014 paper [1].

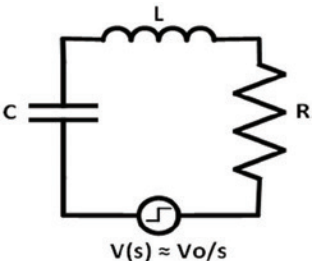

Figure 1: Two-pole RLC model of CDM pulse

For these RLC fits to CDM waveforms, the R^2 (common statistical figure-of-merit) can fall far short of the ideal value of 1.0, sometimes as low as $R^2 < 0.7$ for large targets, representing a very poor fit. Clearly, something else is going on. Many workers have attempted to find clear trends in resistance R (presumed to be the spark resistance) but have not been able to do so. Field simulations of the CDM test fixture impedance have uncovered the expected skin effects, propagation delays, and high-frequency resonances. But, in the end, an L-C approximation holds out to several GHz. Thus, the calculated step response of the fixture and a metal target with constant R (presumably spark resistance) is close to a 2-pole RLC fit because the verification targets in the fixture have a principal resonant frequency of 1-2 GHz or less. The CDM spark itself is therefore thought to cause the observed deviations. Even when the agreement to RLC modeling is close (as can happen for the small target), the inductance L is higher than calculated for the probe and fixture (6-8 nH instead of 4-4.5 nH, for example).

Our recent EOS/ESD Symposium paper [2] discussed this history, including recent attempts to model waveforms with a variable spark resistance R(t), and our own contribution to that. Details and important references are in [2]. We became more comfortable with the idea of inductance built into the spark once we saw some 2021 work about agricultural sparks, which are much larger than semiconductor CDM sparks. In addition, a plot of (electric and magnetic) field energy vs. time for a typical CDM spark (see Figure 2) shows the expected collapse of field energy into the spark followed by a return of some energy to the field at around 1.5-2 nsec. There must be some kind of energy storage (i.e., a reactive element in the spark) for this to happen. The bump does not vanish for any reasonable values of L and C in the CDM test fixture.

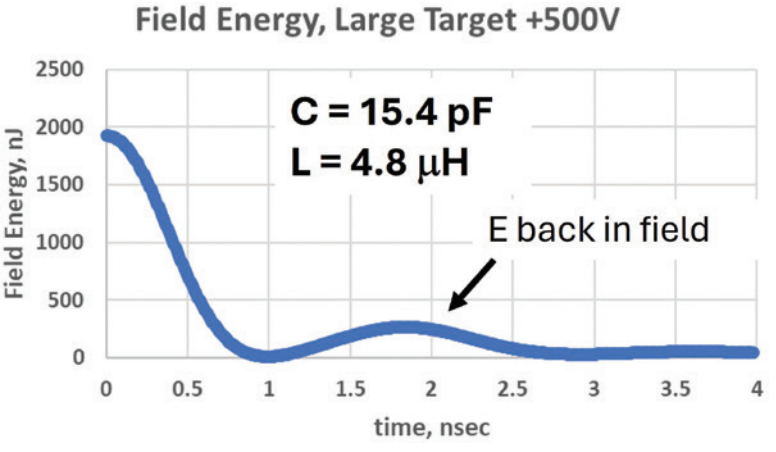

Figure 2: Field energy, $½CV^2 + ½LI^2$, vs. time for large CDM calibration target

The complex frequency s-domain current function for Figure 1 is:

$$I(s) = \frac{CV_o}{LCs^2+RCs+1} \quad (1)$$

where s = σ + jω, and the poles $p_{1,2}$ are such that:

$$p_{1,2} = \omega_o(-D \pm \sqrt{D^2-1}) \quad (2)$$

where $\omega_0 = 1/\sqrt{LC}, D = \omega_0 RC/2$ and is commonly called the damping factor. The waveform will invert into the time domain (Heaviside inversion, in many math books) as a damped sinusoid (D<1), with a complex conjugate pole pair, or as a double exponential (D>1). Our usual case for CDM targets is D<1. But, as indicated above, the large target waveform does not fit the two-pole model of [1,2] very well beyond the first half cycle.

There are essentially two adjustable parameters in Equation 1, since the current can be integrated to give $Q=CV_0$, and C if V_0 is known. If only Q is known, the unitary solution (integral=1) is best expressed through variables ω_0 and D, as follows.

In order to get better fits to our waveforms, and to allow for more reactive circuit elements, we expanded the I(s) current function as simply as possible, by adding a real pole and a real zero:

$$I(s) = \frac{CV_0(1+\tau_2 s)}{(1+\frac{2D}{\omega_0}s+\frac{s^2}{\omega_0^2})(1+\tau_1 s)} \quad (3)$$

Now the 2-pole complex conjugate section of the denominator is expressed with s and s^2 coefficients equivalent to RC and LC, respectively. We call this the three-pole, one-zero (3p1z) model. We now have four parameters, D, ω_0, τ_1, and τ_2, using the standard Heaviside expansion of Equation 3 into time-domain sin, cos, and exp functions, as shown in Equation 4. The fit is readily done in Excel using digital waveforms and Microsoft Solver in GRG (generalized reduced gradient) mode, searching for a least squares minimum, maximizing R^2. More detail is in [2], including how we corrected waveforms for slight cable and oscilloscope losses.

Heaviside expansion into the time domain of a three-pole, one-zero (3p1z) model, such as Equation 3, takes the form:

$$i(t) = Aexp(-at)\cos(bt) + Bexp(-at)\sin(bt) + Cexp(-t/\tau_1) \quad (4)$$

where $a=\omega_0 D$, $b=\omega_0\sqrt{(1-D^2)}$, and A, B, and C are constants driven by total charge CV_0 and on how τ_1 and τ_2 compare. If $\tau_1 = \tau_2$, only the two-pole term B survives. Otherwise, a partial fraction expansion of Equation 3 gives the two-pole term (damped sine), the derivative term (damped cosine), and an exponential term as in Equation 4. For our waveforms, we almost always observed $\tau_1 \geq \tau_2$. This is expected if one decomposes Equation 3 into a 2-pole function modulated by a non-ideal step function, with the step function being:

$$V_0(s) = \frac{V_0(1+\tau_2 s)}{s(1+\tau_1 s)} \quad (5)$$

This is a kind of rise time filter when $\tau_1 > \tau_2$ and helps us understand why rise time filters have been useful for low-impedance contact CDM or LI-CCDM. This is discussed at some length in [2].

We found 3p1z solutions for several dozen waveforms, mostly from small and large CDM verification targets from my co-authors at Intel and Thermo Fisher. R^2 was at least 0.95 and usually well above, and the benefits of two more fitting parameters were clear. Details are in [2]. Next, we sought a one-to-one correspondence between a circuit model and the s-domain expression as in Equation 3. The problem with adding an extra inductor to the circuit in Figure 1 was that $\tau_2 > \tau_1$ was not what we had observed. The key insight was to add an extra capacitor and to allow the extra inductance to be lumped in with the probe and fixture inductance. The new circuit is in Figure 3, with the CDM spark elements on the right-hand side, sharing inductance with the probe and fixture on the left. The 3p1z current function is as follows:

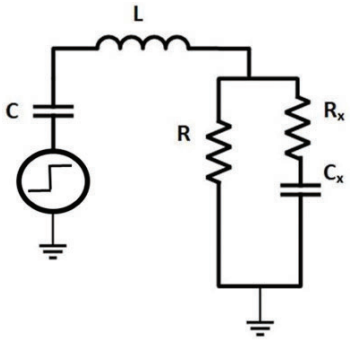

Figure 3: New 3p1z circuit for CDM discharge, with probe, fixture, and metal target on the left sharing inductance with air spark on the right. Total current as in Equation 6.

$$I(s) = \frac{CV_0(1+Cx(R+Rx)s)}{(1+(RC+Cx(R+Rx))s+(LC+RCRxCx)s^2+LCCx(R+Rx)s^3)} \quad (6)$$

The cubic equation in the denominator is not easily factored to find the roots, but we found that, since we have all the coefficients from Equation 3, we wrote out a cubic equation solver in Excel (two complex conjugate roots and one real root for our waveforms) and, once again, used Solver to find an optimal fit. We have C from current integration to $CV_0=Q$, as always, so the four parameters from Equation 3 are fit to circuit elements R, Rx, Cx, and L, in most cases perfectly. If there is any doubt about the partitioning of C and V_0, it can be shown through Equation 6 that C can be chosen arbitrarily and then scaled by α, with αC paired with αCx, L/α, R/α, Rx/α, and V_0/α to give an identical solution. Also, it can be shown that the final inductance L, in Equation 6 and Figure 3, is equal to τ_1/τ_2 times the initial L as in Figure 1 and as would be extracted from Equation 3 ($1/(\omega_0^2 C)$). This inflates the final inductance and can also be thought of as softening the voltage step function, as discussed in [2].

EXAMPLES

Figure 4 shows an example of a large CDM target 3p1z solution and circuit model. The inductor is about twice what we would expect from probe and test fixture, while the extra capacitance Cx almost matches

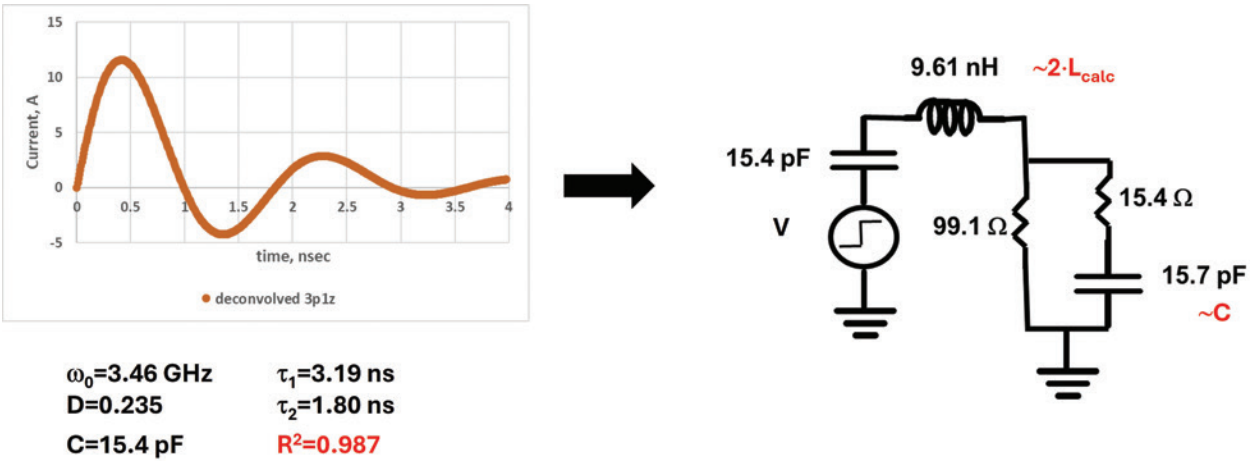

Figure 4: Circuit model and 3p1z parameters for large CDM target, +500V

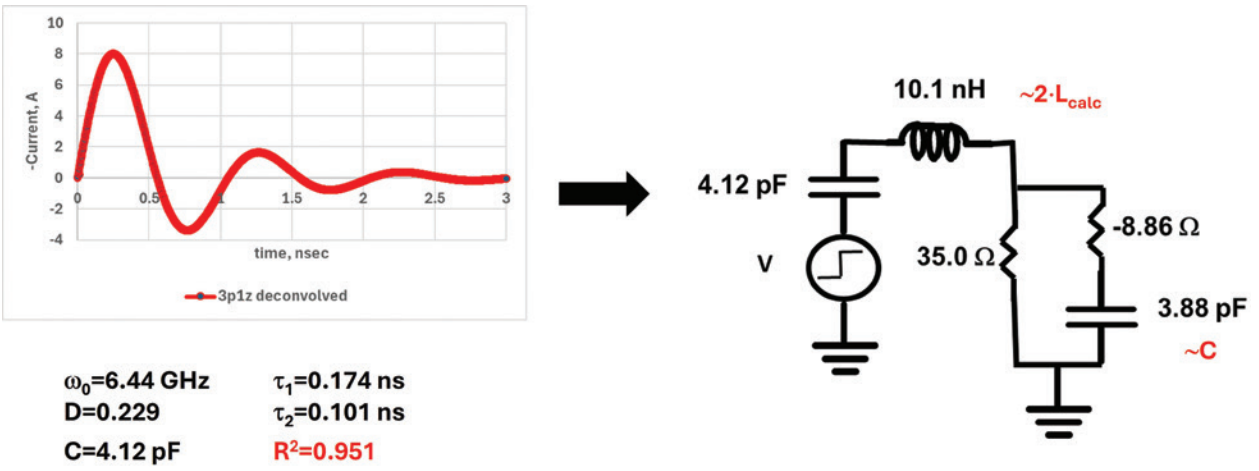

Figure 5: Circuit model and 3p1z parameters for small CDM target, -500V (waveform flipped)

the test fixture capacitance C. The current oscillates initially in the outer loop, where the LC product is about the same as for the test fixture, twice the L and half the C. The spark therefore absorbs the field energy quickly, through L-C matching, and conceals itself, as it were, by ringing at about the frequency expected from the L and C of the probe and target in the test fixture.

Figure 5 shows more of the same for the small target (negative voltage waveform flipped for convenience). Inductance and capacitance "mirroring" in the spark occur again, this time for a much smaller C. Now the Rx in the outer loop is actually negative (not surprising for a plasma), while R=35 ohms bleeds off the spark energy. Despite the negative Rx, the poles and zero of Equation 6 are always in the left half of the complex plane, i.e., stable.

One final case is shown in Figure 6, from the 2023 EOS/ESD Symposium paper 1A.5 [3], data kindly provided by the contributing author [4]. This target was small (1 cm^2) and had a very small probe (inductance about 1 nH), therefore a smaller LC product than usual. Once again there was mirroring of external L and C in the spark itself, this time with negative Rx and even more vigorous high-frequency oscillations (about 3 GHz). This could mean that an air spark plasma resonance becomes more active at higher natural frequencies—if so, it is of strong interest to all CDM situations (factory test socketing, die-to-die (D2D) assembly, etc.) because of the low-inductance packages and interconnects of today.

The CDM test standard (now JS-002) originated in the 1980s when DIP packages justified the 5 mm probe still used in CDM test hardware. The test

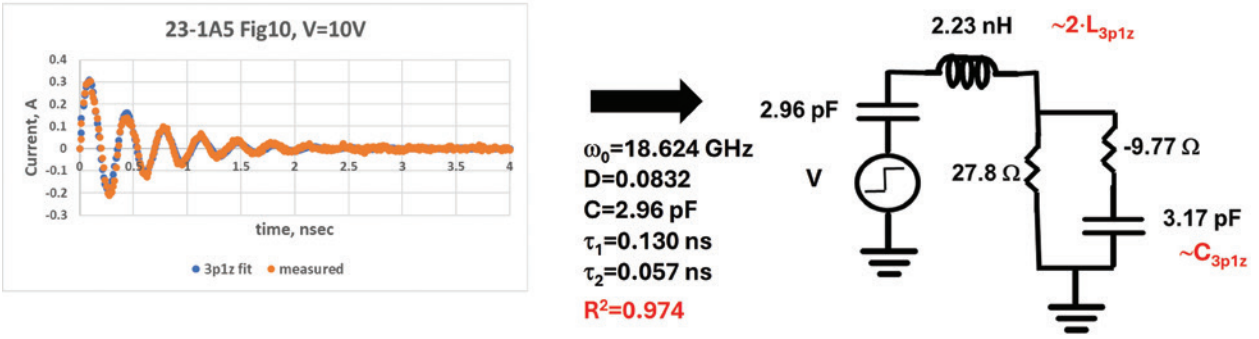

Figure 6: Circuit model and 3p1z parameters for a small, low inductance probe (1 nH) target from a 2023 paper [3], +10V

method has its merits and is not easy to change, but "real" CDM stress events may often have worst-case ringing and currents such as in Figure 6, so we should take note. Waveforms like Figure 6 have been observed at several labs and may represent worst-case CDM conditions.

DISCUSSION AND SUMMARY

As the air spark plasma is composed of excited and ionized atoms and molecules, with lifetimes in the 10s of nanoseconds, plus free electrons, it is not surprising that energy-storage elements (extra inductance and, usually, capacitance) are part of the spark circuit model. Also, voltage is expected to precede plasma current flow, the I-V phase relation of an inductor. Remarkably, the spark's extra L and C are usually a near-match for the L and C of the external environment, assuring a quick flow of energy into the spark from the field. The thermodynamics of this process could be interesting to study.

This initial work on the CDM spark circuit model should be continued on to larger and smaller target (i.e., package) sizes, and varying probe inductance so that the variety of CDM test and use conditions is comprehended. At some point, trends for all the circuit elements should be clear enough that the circuit model for any metal target (akin to a short circuit) in any CDM environment can be predicted, and with it trends for peak current and such. The model can then, for example, be used as a CDM "source," surrounding a known ESD circuit model of a pin under test.

To facilitate the exploratory studies of these various CDM test conditions, the algorithm described here and in [2] could be ported to a software platform where the circuit parameters are found after very few keystrokes, as with existing ESD waveform evaluation software for human body model (HBM). Also, now that we have a circuit topology for the spark, we can imagine using a licensed version of SPICE simulator that finds optimized circuit element values given a topology. Having made fast work of the waveform evaluation, we can expect considerable physical insight to emerge from the trends discernable from large amounts of CDM data, much of which is already on file.

Finally, we should see if air spark plasma conditions produce the occasional high-frequency resonance (Figure 6) when certain external L-C conditions are met. This could represent a worst case for CDM peak current in factory assembly/test or D2D conditions. If the idea of an avalanche process and drift time of carriers to anode/cathode resonating with an external circuit sounds familiar to an electrical engineer, it could be because the decades-old high-power microwave IMPATT diode (impact ionization avalanche transit time) works on exactly that principle. We should find out if the occasional occurrence of such conditions is a threat to our devices in manufacturing and protect them accordingly.

REFERENCES

1. T. Maloney and N. Jack, "CDM Tester Properties as Deduced from Waveforms," IEEE TDMR-14, pp. 792-800. https://bit.ly/2VQlUfQ
2. T. Maloney, P. Ensaf, and M. Hernandez, "Intrinsic Inductance and Time-Dependent Resistance of the FI-CDM Spark," 2024 EOS/ESD Symposium Proceedings, paper 2B.3, pp.93-102. Paper and slides at https://bit.ly/3WV9nod, slides presented at https://youtu.be/Oa5BQVCFBAo.
3. D. Johnsson, P. Tamminen, D. Oy, T. Viheriakoski, H. Gossner, "Discharge Waveforms of Emulated Die-to-Die ESD Discharges," 2023 EOS/ESD Symposium Proceedings, paper 1A.5, pp. 47-55. https://doi.org/10.23919/EOS/ESD58195.2023.10287762
4. P. Tamminen, private communication.

CAPACITOR IMPEDANCE EVALUATION FROM S-PARAMETER MEASUREMENTS

Part 1: S_{11} One-Port Shunt, Two-Port Shunt and Two-Port Series Methods

By Bogdan Adamczyk, Patrick Cribbins, and Khalil Chame

This is the first of two articles devoted to the topic of capacitor impedance evaluation from the *s* parameter measurements using a network analyzer. Part 1 describes the impedance measurements and calculations from the s_{11} parameter using the one-port shunt method, two-port shunt, and two-port series methods. Part 2 will discuss impedance measurements and calculations using the s_{21} parameter with two-port shunt and two-port series methods.

Dr. Bogdan Adamczyk is professor and director of the EMC Center at Grand Valley State University (http://www.gvsu.edu/emccenter) where he performs EMC educational research and regularly teaches EM/EMC courses and EMC certificate courses for industry. He is an iNARTE-certified EMC Master Design Engineer. He is the author of two textbooks, "Foundations of Electromagnetic Compatibility with Practical Applications" (Wiley, 2017) and "Principles of Electromagnetic Compatibility: Laboratory Exercises and Lectures" (Wiley, 2024). He has been writing "EMC Concepts Explained" monthly since January 2017. He can be reached at adamczyb@gvsu.edu.

Patrick Cribbins is pursuing his Bachelor of Science in Electrical Engineering at Grand Valley State University. He currently works full time as an Electromagnetic Compatibility Engineering co-op student at E3 Compliance, which specializes in EMC and high-speed design, pre-compliance testing and diagnostics. He can be reached at patrick.cribbins@e3compliance.com.

Khalil Chame is pursuing his Bachelor of Science in Electrical Engineering at Grand Valley State University. He currently works full time as an Electromagnetic Compatibility Engineer co-op student at E3 Compliance, which specializes in EMC and high-speed design, pre-compliance and diagnostics. He can be reached at khalil.chame@e3compliance.com.

CONFIGURATIONS, CIRCUIT MODELS, S_{11} – IMPEDANCE RELATIONSHIPS

One-Port Shunt Method

Note: The one-port shunt method is also called a (one-port) reflection method [1]. One-port configuration for a two-terminal DUT is shown in Figure 1.

Figure 2 shows the transmission line circuit model at Port 1.

The network analyzer sends the incident waves (at different frequencies) to Port 1, terminated with Z_x (interconnects are taken out of the measurements through the calibration process).

Upon the arrival at load Z_x, the incident waves get reflected (unless the load impedance Z_x equals Z_0). The reflected voltage waves, v_r, are related to incident voltage waves, v_i, by the load reflection coefficient, Γ, defined as

$$\Gamma = \frac{v_r}{v_i} \quad (1)$$

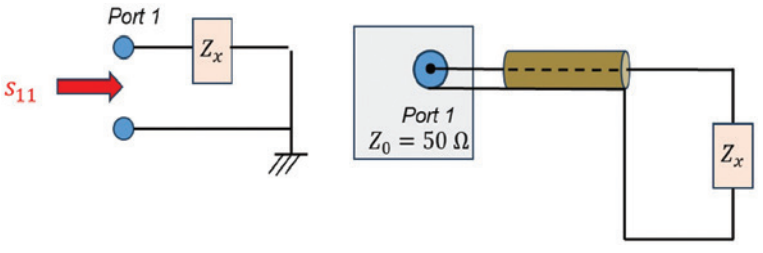

Figure 1: One-port shunt configuration

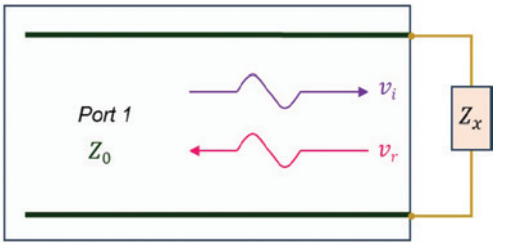

Figure 2: Transmission line circuit model of one-port shunt configuration

This load reflection coefficient equals the s_{11} parameter and can be computed from [2],

$$s_{11} = \Gamma = \frac{Z_x - Z_0}{Z_x + Z_0} \quad (2)$$

Eq. (1) is used to obtain the DUT impedance in terms of s_{11} parameter, as follows

$$s_{11}(Z_x + Z_0) = Z_x - Z_0 \quad (3)$$

$$s_{11}Z_x + s_{11}Z_0 = Z_x - Z_0 \quad (4)$$

$$s_{11}Z_0 + Z_0 = Z_x - s_{11}Z_x \quad (5)$$

$$Z_0(s_{11} + 1) = Z_x(1 - s_{11}) \quad (6)$$

Resulting in the DUT impedance in terms of the s_{11} parameter as [1],

$$Z_x = Z_0 \frac{1 + s_{11}}{1 - s_{11}} \quad (7)$$

Two-Port Shunt Method

The two-port shunt configuration for a two-terminal DUT is shown in Figure 3.

The simplified circuit model of this shunt configuration is shown in Figure 4.

Note that the DUT impedance Z_x is in parallel with the Port 2 impedance Z_0, resulting in an equivalent load impedance of

$$Z_L = \frac{Z_x Z_0}{Z_x + Z_0} \quad (8)$$

The s_{11} parameter equals the load reflection coefficient and can be computed from

$$s_{11} = \Gamma = \frac{Z_L - Z_0}{Z_L + Z_0} \quad (9)$$

Utilizing Eq. (8) in Eq. (9) we get

$$s_{11} = \frac{\frac{Z_x Z_0}{Z_x + Z_0} - Z_0}{\frac{Z_x Z_0}{Z_x + Z_0} + Z_0} \quad (10)$$

or

$$s_{11} = \frac{Z_x Z_0 - Z_0(Z_x + Z_0)}{Z_x Z_0 + Z_0(Z_x + Z_0)} \quad (11)$$

$$s_{11} = \frac{-Z_0^2}{2Z_x Z_0 + Z_0^2} \quad (12)$$

which simplifies to

$$s_{11} = \frac{-Z_0}{2Z_x + Z_0} \quad (13)$$

Eq. (13) is now solved for Z_x in terms of s_{11}.

$$s_{11}(2Z_x + Z_0) = -Z_0 \quad (14)$$

or

$$2Z_x s_{11} + Z_0 s_{11} = -Z_0 \quad (14)$$

$$2Z_x s_{11} = -Z_0 - Z_0 s_{11} \quad (15)$$

$$2Z_x s_{11} = -Z_0(1 + s_{11}) \quad (16)$$

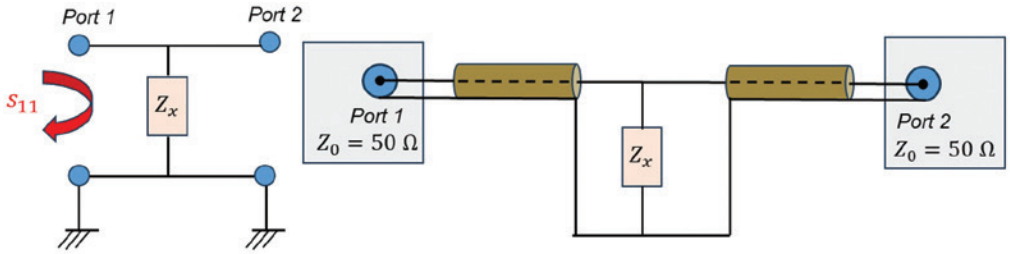

Figure 3: Two-port shunt configuration

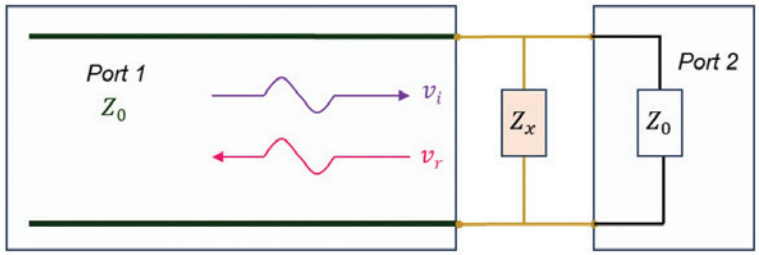

Figure 4: Transmission line circuit model of two-port shunt configuration

resulting in

$$Z_x = -Z_0 \frac{1+s_{11}}{2s_{11}} \quad (17)$$

Two-Port Series Method

The two-port series configuration for a two-terminal DUT is shown in Figure 5.

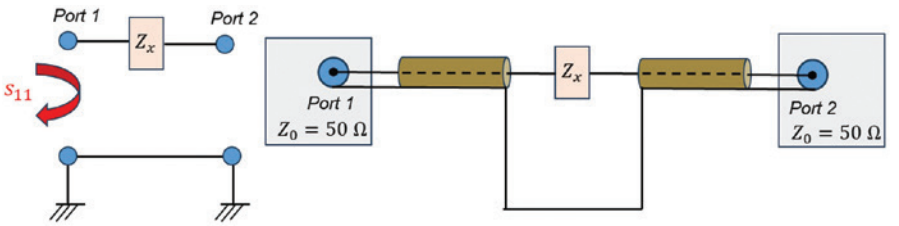

Figure 5: Two-port series configuration

The simplified circuit model of this series configuration is shown in Figure 6.

Note that the DUT impedance Z_x is in series with the Port 2 impedance Z_0, resulting in an equivalent load impedance of

$$Z_L = Z_x + Z_0 \quad (18)$$

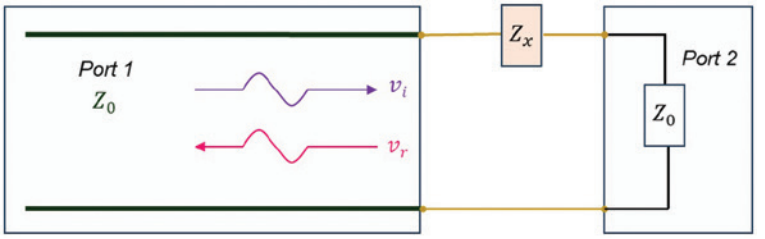

Figure 6: Transmission line circuit model of two-port series configuration

The s_{11} parameter equals the load reflection coefficient and can be computed from

$$s_{11} = \Gamma = \frac{Z_L - Z_0}{Z_L + Z_0} \quad (19)$$

Utilizing Eq. (18) in Eq. (19) we get

$$s_{11} = \frac{Z_x + Z_0 - Z_0}{Z_x + Z_0 + Z_0} \quad (20)$$

or

$$s_{11} = \frac{Z_x}{Z_x + 2Z_0} \quad (21)$$

Eq. (21) is now solved for Z_x in terms of s_{11}.

$$s_{11}(Z_x + 2Z_o) = Z_x \quad (22)$$

or

$$Z_x s_{11} + 2Z_0 s_{11} = Z_x \quad (23)$$

$$2Z_0 s_{11} = Z_x - Z_x s_{11} \quad (24)$$

$$2Z_0 s_{11} = Z_x(1 - s_{11}) \quad (25)$$

resulting in

$$Z_x = 2Z_0 \frac{s_{11}}{1 - s_{11}} \quad (26)$$

IMPEDANCE MEASUREMENT SETUP AND RESULTS

The impedance measurement setup and the PCB boards are shown in Figure 7. The boards were populated with Murata X7R ceramic capacitors, GCM188R71H472KA37, GCM188R71H473KA55, GCM188R71C474KA55, of the values 4.7 nF, 47 nF, and 470 nF, respectively.

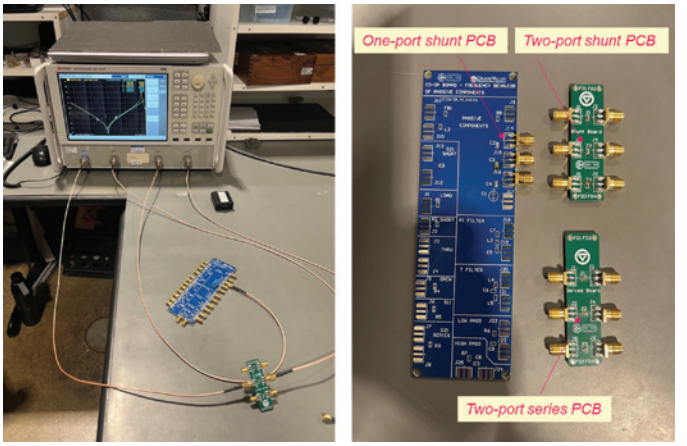

Figure 7: Measurement setup and PCBs

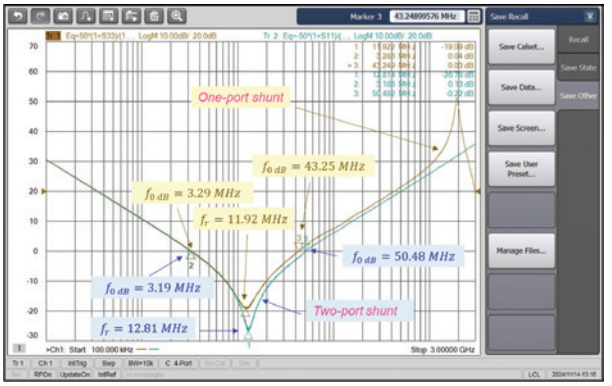

Figure 8: S_{11}-based impedance curves - one-port shunt (Eq. 7) vs. two-port shunt (Eq. 17)

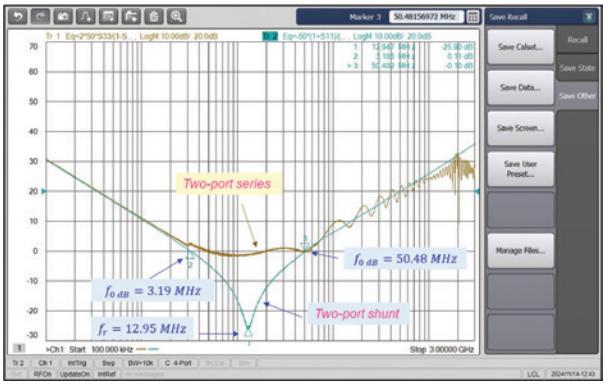

Figure 9: S_{11}-based impedance curves - two-port series (Eq. 26) vs. two-port shunt (Eq. 17)

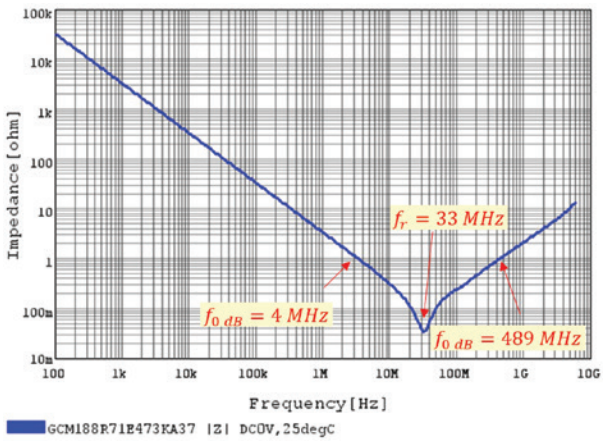

Figure 10: Murata "SimSurfing" impedance curve for 47 nF capacitor

Impedance curves for a *47 nF* capacitor are shown in Figures 8 and 9. Figure 8 compares the results between the one-port shunt and two-port shunt configurations, while Figure 9 compares the two-port series and two-port shunt configurations.

Clearly, the two-port series measurement is not reliable. Figure 10 shows the capacitor impedance curve obtained from the Murata Design Support Software "SimSurfing" [3].

The one-port shunt, two-port shunt and Murata measurements at 0 dB and at self-resonant frequencies are shown in Table 1.

Clearly, the one-port shunt and two-port shunt measurements do not agree with the Murata values. The measurement results for the other two capacitors (4.7 nF, 470 nF), not presented here, showed similar trends.

The overall conclusion is that the capacitor impedance evaluation from s_{11} parameter measurements is not accurate. The next article will discuss the capacitor impedance estimation from s_{21} parameters and show its superiority over the s_{11}-based methods.

REFERENCES

1. Microwaves & RF Application Note, *Make Accurate Impedance Measurements Using a VNA*. https://www.mwrf.com/technologies/test-measurement/article/21849791/copper-mountain-technologies-make-accurate-impedance-measurements-using-a-vna
2. Keysight Application Note, *Impedance Measurements of EMC Components with DC Bias Current*. https://www.keysight.com/us/en/assets/7018-01969/application-notes/5989-9887.pdf
3. Murata Design Support Software "SimSurfing." https://ds.murata.co.jp/simsurfing/index.html?lcid=en-us

	One-port shunt	Two-port shunt	Murata
1st 0 dB frequency	3.29 MHz	3.19 MHz	4 MHz
Resonant frequency	11.92 MHz	12.81 MHz	33 MHz
2nd 0 dB frequency	43.25 MHz	50.48 MHz	489 MHz

Table 1: Impedances at 0 dB and self-resonant frequencies

UNDERSTANDING ESD CONTROL

Part 1: Charge Buildup and Resistance to Ground

Dr. Jeremy Smallwood on behalf of EOS/ESD Association, Inc.

The normal world is full of electrostatic discharge (ESD) risks to unprotected ESD susceptible devices (ESDS). To handle these, we must set up an ESD Protected Area (EPA) in which we have reduced the ESD risks to a low level. In Part 1, this article will look at how static electricity works. Part 2 will look at how we control it in an EPA.

Dr. Jeremy Smallwood has worked in electrostatics and ESD control since the late 1980s. He formed Electrostatic Solutions Ltd. in 1998 to provide electrostatics consultancy, training, and R&D services for industry and works with British and IEC standards Committees. His book "The ESD Control Program Handbook" was published by Wiley in 2020.

Where does static electricity come from? Science tells us that every material is made of atoms. Atoms are made of electrical charges – positive protons in the atomic nucleus and negative electrons around them. When these are present in equal numbers, their electrical effects cancel.

When two materials touch, some charges move from one material to the other. When the materials separate, each takes a small surplus of one type of charge. Repetition can build the charge imbalance. The charges will try to move to restore balance if they can, but if prevented – static electricity starts to accumulate.

These processes happen very easily. Several thousand volts can be measured on the surface of a plastic sheet lifted from a pile of materials. Packing tape pulled from the reel can give readings of tens of thousands of volts. The repeated shoe-floor contact of a person walking can raise their body to several thousand volts – when they discharge by touching something, they get a shock, as most of us have experienced.

The buildup of charge is rather like the buildup of water in a wash basin. A basin has a tap that allows water in and a drain that lets water out. If there is no plug in the drain, and only a small amount of water flows in, it can run out as fast as it enters with no buildup. Similarly, if charge can flow away (dissipate) as quickly as it is separated, there is no buildup of static electricity. If, however, the basin has a partly blocked or small drain and the tap is full-on, the water level in the basin can build up. If a basin has a blocked drain or the plug is in the plughole, it only needs a dripping tap to cause water level buildup. Similarly, if charge cannot dissipate, only a small amount of charge separation can lead to a buildup of charge and high voltage levels.

INSULATORS AND CONDUCTORS

The materials that act like the plug in the plughole are insulators. An insulator is a material that does not allow charge to move away quickly enough to avoid charge buildup. These are materials like ordinary plastics and rubber. Insulators promote charge buildup and ESD risks, so we prefer not to have them near ESDS in an EPA.

Any item which is not an insulator allows charge to move around quickly enough to avoid charge buildup, providing the charge has somewhere to go. These are the conductors, static dissipative, and conductive materials. The IEC 61340-5-1 and ANSI/ESD 20.20 standards have specific definitions, classifying an insulator as a material or item having resistance over 100 GΩ (10^{11} Ω) and a conductor as an item or material with resistance less than 10 kΩ. "Static dissipative" items and materials are those with intermediate resistance. Be careful – not all industries and standards use the same definitions. Examples of conductors and static dissipative materials can be metals, ESD control materials and water. The human body is mainly water and has resistance between about 1 kΩ and 100 kΩ depending on many factors.

IEEE ISPCE 2025

IEEE International Symposium on Product Compliance Engineering

MAY 13-15, 2025 || SAN FRANCISCO, CA, USA

ABOUT THE CONFERENCE

Experience three days of educational workshops and technical presentations given by the industry experts focusing on pertinent topics concerning Product Safety, Certifications, and Global Compliance.

The First 150 early bird registrations will receive a FREE 3-day Trolley Cable Car Passport with unlimited rides, including any Muni transportation!

Register before February 14 to receive a discounted rate!

TOP 6 TOPICS PRESENTED AT ISPCE:

- Cybersecurity
- EMC & Wireless Compliance
- Global Hazardous Locations
- Global Market Access
- Product Safety Compliance
- Artificial Intelligence (AI) for Product Compliance

For more information on how to register please visit us online at 2025.psessymposium.org/registration.

A LITTLE THEORY….

Simple circuits can be used to help understand how static electricity works and how ESD control can be established. Many situations can be simply modeled as a current generator I (charge separation), feeding into some charge storage (capacitance C, the potential ESD source) and leakage (resistance R_g). One side of C and R_g are often earth – in ESD control this can be the common point ground. Charge is partly stored in C and, at the same time partly leaks away through R_g.

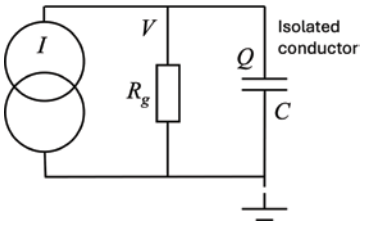

If the voltage V is constant, from Ohm's Law

$$V = IR_g$$

If the charging current I = 10 nA and R_g = 1 GΩ, then V is only 10 V, which would not usually be noticed as static electricity. However, if R_g is 1000 GΩ, V would be 10 kV, which would likely be noticed, with a strong possibility of ESD occurring. So, the maximum resistance (usually resistance to ground) effectively sets the maximum voltage generated by a given charging current.

The parallel resistance R_g and capacitance C define a time constant, the product $R_g C$. If charge generation stops, the charge stored in C flows through R_g and an exponential decay of voltage V occurs. V drops to 5 % of its initial value in 3 x $R_g C$. If, for example, C = 100 pF (10^{-10} F, e.g., a charged person) and R_g is 1 GΩ (10^9 Ω), the product $R_g C$ is 0.1 seconds – the voltage drops within a second and would not be noticed. If R_g were 100 GΩ in the same circumstance, the voltage decay time would be 10 seconds - long enough to potentially cause a problem. So, a second important effect of limiting the maximum resistance can be to keep the charge dissipation time short.

Another important factor is atmospheric humidity. We're all familiar with the condensation that often forms on our cold drink glass – this, of course, comes from moisture in the air. Similarly, many materials have a very thin surface moisture layer that can provide a path for charge to dissipate. It tends to be thicker and has lower electrical resistance when the air humidity is higher. Below about 30% RH, the moisture layer breaks up and charge dissipation is inhibited. Materials and items tend to charge more easily below 30 % RH, but at high RH, it can be difficult to generate electrostatic charge.

In ESD control, we replace insulators with conductive or static dissipative materials where possible and provide a path for the charge to dissipate. Any charged conductor can act as an ESD source, so we usually set a maximum resistance to ground R_g to limit voltage buildup in expected situations and reduce the time taken to dissipate charge. If R_g is too high, the voltages generated by charging currents can be too high, and the charge dissipation time can be too long. Providing these controlled dissipation paths largely removes any reliance on moisture from atmospheric humidity in controlling charge buildup. If we specify our materials to give low enough resistance at low humidity, humidity becomes irrelevant.

In Part 2, we'll look at how resistance in the discharge path when ESD occurs can have a protective effect and how these ideas are applied in practical ESD control.

REFERENCES AND FURTHER READING

1. International Electrotechnical Commission, *Electrostatics – Part 5-1: Protection of electronic devices from electrostatic phenomena - General requirements*, IEC 61340-5-1.
2. ESD Association, *ESD Association Standard for the Development of an Electrostatic Discharge Control Program for – Protection of Electrical and Electronic Parts, Assemblies and Equipment (excluding Electrically Initiated Explosive Devices),* ANSI/ESD S20.20-2021.
3. Smallwood J. M., *The ESD Control Program Handbook*, Wiley, 2020, ISBN 978 1 118 31103-5.

ABOUT THE EOS/ESD ASSOCIATION, INC.

Founded in 1982, EOS/ESD Association, Inc. is a not for profit, professional organization, dedicated to education and furthering the technology Electrostatic Discharge (ESD) control and prevention. EOS/ESD Association, Inc. sponsors educational programs, develops ESD control and measurement standards, holds international technical symposiums, workshops, tutorials, and foster the exchange of technical information among its members and others.

MEASURING AND REDUCING GROUND BOUNCE IN A LARGE DRIVE SYSTEM

By Dr. Min Zhang

Electromagnetic interference (EMI) issues that engineers encounter in the field are often due to poor layout design, with grounding layout problems being one of the primary contributors. From a radio frequency (RF) perspective, even a path with seemingly low resistance can present significant impedance. When RF currents are forced through this high-impedance path, a substantial RF voltage difference can develop. This voltage difference across what should be a common low-impedance ground can elevate noise levels.

This issue arises at both the printed circuit board (PCB) level and the system level. In this month's column, we examine system-level troubleshooting techniques commonly used to identify grounding issues. We also demonstrate how improvements to system grounding can effectively reduce noise.

In this case study, the equipment under test (EUT) is a bi-directional power converter that uses two IGBT-based drive systems to deliver large bursts of power for mission-critical applications. As shown in Figure 1, we set up an on-site conducted emission test using a 32A three-phase LISN. Figure 1 also displays the initial conducted emission scanning results, showing several frequency bands where the EUT failed to meet compliance.

It didn't take long to identify that resonance peaks in the lower frequency range (300 - 400 kHz) were due to insufficient filtering on both the input and output ports of the EUT. The client had initially chosen three-phase, three-wire EMI filters, allowing the neutral line to carry a significant amount of low-frequency common-mode current, effectively bypassing the filters. The solution here is to replace these three-phase, three-wire EMI filters with three-phase, four-wire versions.

Dr. Min Zhang is the founder and principal EMC consultant of Mach One Design Ltd, a UK-based engineering firm that specializes in EMC consulting, troubleshooting, and training. His in-depth knowledge in power electronics, digital electronics, electric machines, and product design has benefitted companies worldwide. Zhang can be reached at info@mach1desgin.co.uk.

While we waited for the new filters to arrive, there was still another noise issue to address at around 2 MHz, caused by a different resonance source. This noise could not be mitigated even with a three-phase four-wire filter, requiring an entirely different approach to address it. Upon reviewing the system design, we found that both motor drives were located in one inner compartment, connected via wires to the magnetics compartment, which contains the low-frequency choke, capacitors, transformers, and EMI filters. We questioned whether the ground difference (or ground bounce) between the drive and magnetics compartments could be contributing to the noise at 2 MHz.

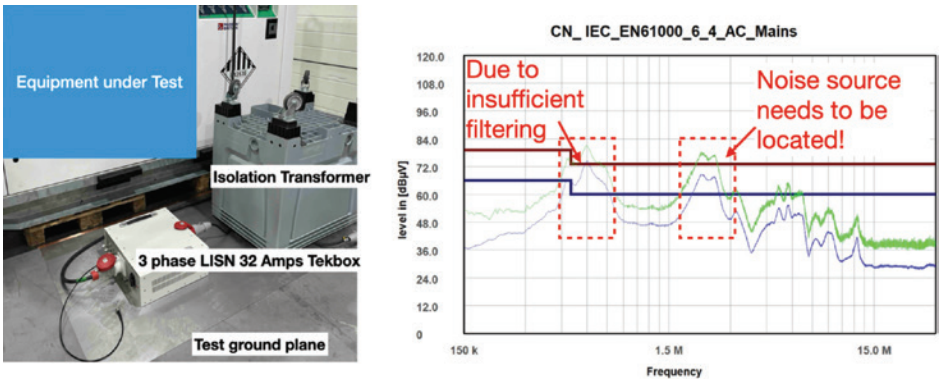

Figure 1: Pre-compliance conducted emission set-up and initial results

To investigate this, we measured the ground potential difference. Although several tools are available for measuring noise in this frequency range (after all, it is only 2 MHz),[1] we opted for the Onfilter Power Line EMI Adapter.[2,3] This adapter provides complete galvanic isolation from high mains voltages while allowing a direct path for high-frequency signals. This setup enabled us to connect our sensitive instruments to live power lines safely and measure EMI between different grounded parts without creating ground loops.

In Figure 2, we conducted the measurement by tapping the probe tips between the two grounding points in question. Measurements in both the time and frequency domains confirmed that this ground difference contributed to the noise observed at 2 MHz.

Once we verified this with measurements, the solution became clear: improve the grounding between the two compartments. As shown in Figure 3, we could not use short braided wire as the mechanical design was not easy to change, so we added multiple ground leads. With each additional cable between the compartments, we observed a reduction in ground differential, ultimately almost halving the noise (8V peak to peak compared with 15V peak to peak).

Further improvement came from using a shielded cable screen to connect the compartments, which achieved a comfortable pass in the targeted frequency range (2 MHz).

ENDNOTES

1. Min Zhang, *Signal Integrity Journal*, "Troubleshooting Low Frequency Common Mode Emissions," February 1, 2023.
2. Ken Wyatt, the EMC blog, *EDN*, "Review: Tool Measures Power-line EMI," November 25, 2020.
3. Power Line EMI Adapter MSN15 https://www.onfilter.com/emi-adapter-msn15

Figure 2: We measured the ground bounce; results are shown in both time and frequency domains

Figure 3: We improved the grounding structure between the compartments; results showed improvement in both time and frequency domain

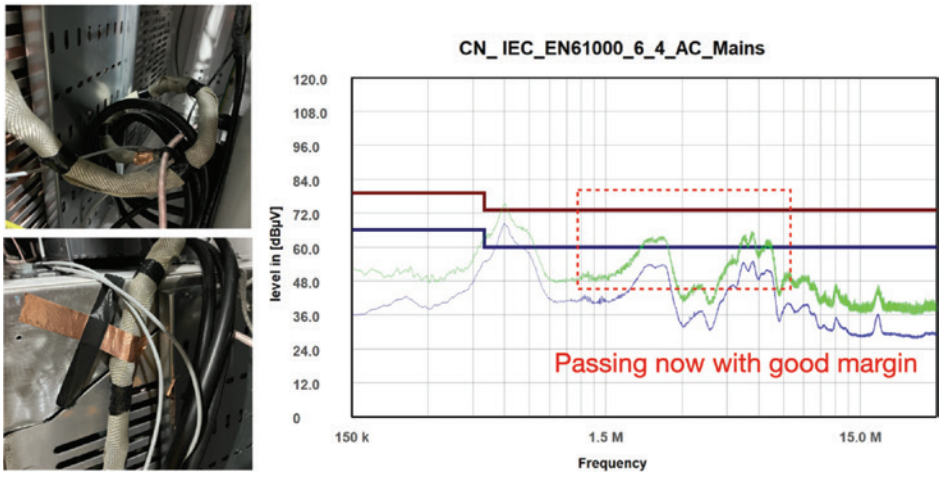

Figure 4: Using shielded cable further reduced the noise at 2 MHz

PRODUCT Showcase

The EERC™

Electrical Engineering
Resource Center

calculator

offered by A.H. Systems, Inc.

Antenna Factor and Gain Calculations

Transform complex antenna measurements into instant results with this essential calculator. Convert between Antenna Factor (dB/m) and Gain (dBi) values effortlessly. Save valuable engineering time and eliminate calculation errors with this streamlined tool designed for RF professionals and researchers.

https://incompliancemag.com/EERC

Advertiser Index


OPHIR RF
THE ART OF WIRELESS™
High Power RF Systems
For Radiated Immunity Testing
Frequency 10 KHz-40 GHz And Beyond
VSWR Tolerant Designs
Power Levels To 20 kW And Beyond
5 Year Warranty
www.OphirRF.com
Los Angeles, California
SINCE 1992

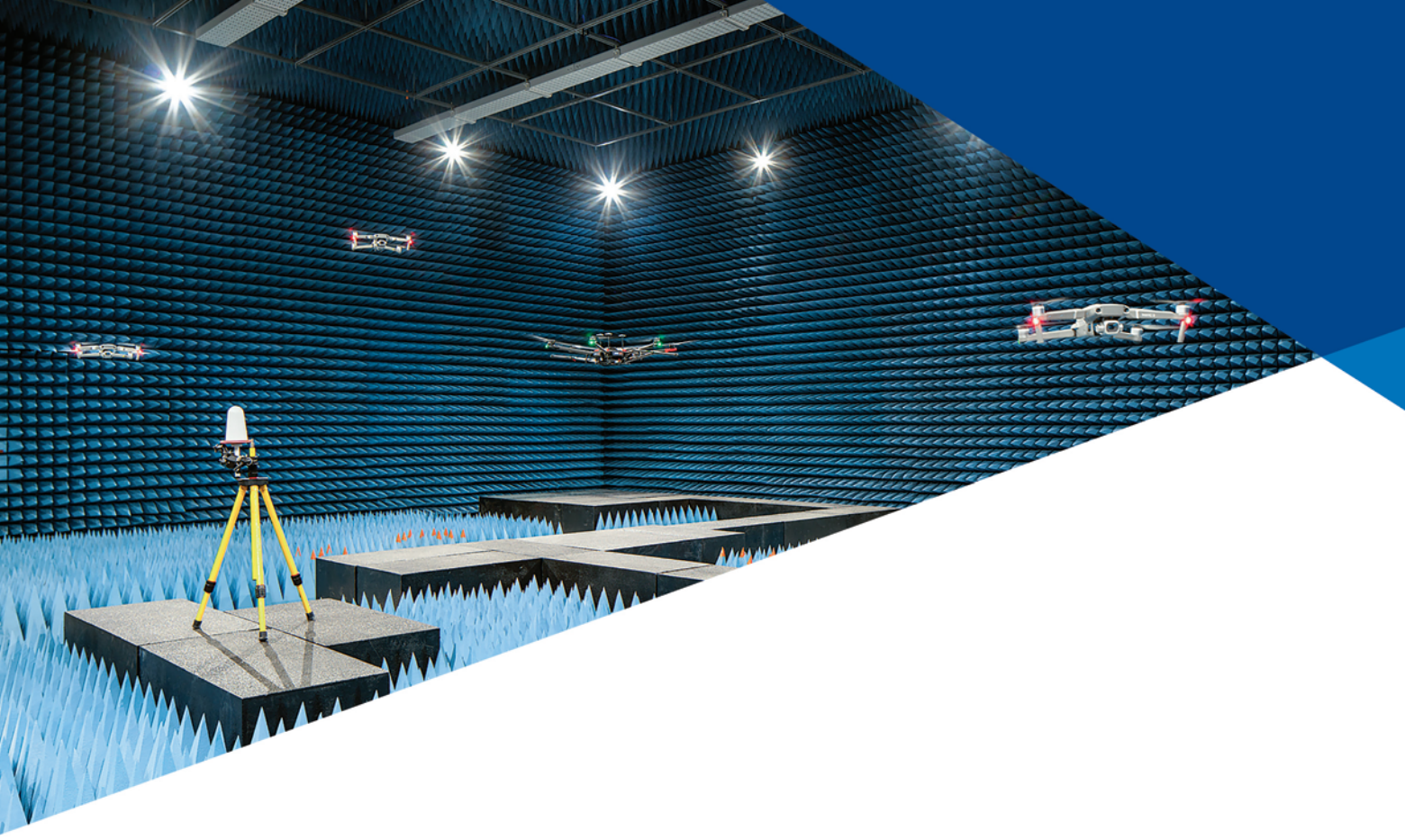

SHAPE THE FUTURE OF ANTENNAS AND PROPAGATION WITH ETS-LINDGREN.

When it comes to cutting-edge Wireless, RF, and Microwave Test Systems, ETS-Lindgren leads the way. As the global authority in innovative test solutions, we deliver unmatched performance and reliability for far-field, near-field, and compact range chambers, designed for RCS and antenna measurement testing. Our solutions are trusted worldwide by leading organizations in the automotive, defense/aerospace, and wireless industries.

With over 50,000 installations globally, ETS-Lindgren is the preferred partner for turnkey systems that ensure precision and dependability. Our vertically integrated approach means we produce 90% of a project's components in-house—from RF Shielded Enclosures and Absorbers to Multi-Axis Positioners, custom-designed Antennas, and advanced Software—ensuring unparalleled quality and seamless integration.

Our comprehensive services include:

- Builder of the World's Largest Anechoic Chamber
- Provider of 80% of CTIA Authorized Test Labs (CATLs) Worldwide
- Innovator of Countless Industry-First Advancements

Join the ranks of international clients who trust ETS-Lindgren to push the boundaries of what's possible. Together, we'll redefine the future of antennas and propagation. For more information on our solutions, visit www.ets-lindgren.com or contact your local ETS-Lindgren office or representative.

Connect with us at:

COMMITTED TO A SMARTER, MORE CONNECTED FUTURE

ETS·LINDGREN®
An ESCO Technologies Company

Offices Worldwide | **ets-lindgren.com**